

# Angular Momentum in Turns and Abrupt Starts: Strategies for Bipedal Balance Control

by

Matthew Todd Farrell

B.A. Mathematics  
Bard College at Simon's Rock, 2004

Submitted to the Program in Media Arts and Sciences,  
School of Architecture and Planning,  
in partial fulfillment of the requirements for the degree of  
Master of Science

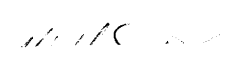
at the

MASSACHUSETTS INSTITUTE OF TECHNOLOGY

May 2009

©Massachusetts Institute of Technology 2009. All rights reserved.

AUTHOR: Program in Media Arts and Sciences  
Associate Professor of Media Arts and Sciences

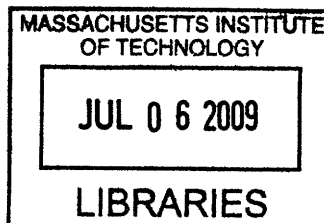
  
\_\_\_\_\_  
(SIGNATURE OF AUTHOR)

CERTIFIED BY: Professor Hugh Herr  
Professor of Media Arts and Sciences  
Thesis Supervisor

\_\_\_\_\_  
(SIGNATURE OF ADVISOR)

ACCEPTED BY: Professor Deb Roy  
Chair, Program in Media Arts and Sciences

\_\_\_\_\_  
(SIGNATURE OF CHAIR)



**ARCHIVES**

# Angular Momentum in Turns and Abrupt Starts: Strategies for Bipedal Balance Control

by

Matthew Todd Farrell

B.A. Mathematics  
Bard College at Simon's Rock, 2004

Submitted to the Program in Media Arts and Sciences,  
School of Architecture and Planning,  
in partial fulfillment of the requirements for the degree of  
Master of Science

## Abstract

Transients occur in human walking during a transition to, from, and between steady state walking and act as an impulse destabilizing an otherwise normal gait cycle. Turns and accelerated starts are all common transients encountered and managed intelligently by humans everyday. The population of elderly has increased and understanding balance control in healthy subjects will be more important. In addition, humanoid bipeds are rapidly becoming a more common part of our everyday life. Therefore, they must also be able to navigate our environments adroitly if they are to assist us in our daily living. This thesis takes biomechanical principals of angular momentum and applies them to healthy subjects in an effort to elucidate human balance control strategies. Each transient task is unique, and despite large segmental contributions to whole-body angular momentum during movement, the whole-body angular momentum remains tightly regulated. A analysis of segmental contributions to the principal components explaining more than 90% makes clear the balance control strategy used by healthy humans during these transients.

Thesis Supervisor: Hugh Herr

Title: Associate Professor of Media Arts and Sciences


# Angular Momentum in Turns and Abrupt Starts: Strategies for Bipedal Balance Control

by


Matthew Todd Farrell

The following people served as readers for this thesis:

READER ONE: Professor Russ Tedrake  
Assistant Professor of Electrical Engineering  
and Computer Science

  
\_\_\_\_\_  
(SIGNATURE OF READER)

READER TWO: Professor Joeseeph Paradiso  
Professor of Media Arts and Sciences

  
(SIGNATURE OF READER)

## Acknowledgements

This thesis is the result of many discussions, long hours, and the active participation and help from several people from around MIT. Without them, this thesis could not have been completed and indeed neither could this work have begun in the first place.

Thank you to Marko Popovic for introducing me to this field. Also, Professor Hugh Herr for being my advisor and supporting me through my thesis. Also, thank you to my lab-mates without whom I would not have been able to complete my work; especially through the long discussions and participating in my experiments.

I would like to thank my father in particular. Throughout my life he has provided guidance, love and support for me in making the hardest decisions in my life. He is my conscience and constantly asking me to question everything around me. Without him I would never have made it this far.

My mother has always been behind me through many ups and downs. She has provided the support and confidence I needed, when I needed it, to see through the difficult challenges in my life. Always, she gives me a goal to strive for and the desire for a life more extraordinary.

Without my family I would be nothing.

Thank you to my family and friends for their support and help throughout the time leading up to and during my degree. Xiao Xiao, thank you for putting up with all my frantic late nights. Thank you to Ken Endo and Ernesto Martinez for so much advice and wisdom.

On to the next degree...

## Contents

Acknowledgements	4
List of Figures	7
List of Tables	11
Chapter 1. Introduction	13
1. Outline of Thesis	13
2. Societal Motivation and Demand	15
3. Problem Statement	16
Chapter 2. Background	19
1. Previous Work	19
2. Ground Reference Trajectories	21
Chapter 3. Experimental Methods	25
1. Human Subject Experiments	25
2. Force Plates Details	27
3. Motion Capture Details	29
4. Data Analysis Pipeline	30
Chapter 4. Analytical Methods	33
1. Human Model	33
2. Horizontal ground reaction force predictions	36
3. Segmental contributions to the whole-body angular momentum	39
Chapter 5. Results	45
1. Normal Walking in Sagittal Plane	45
2. Left Inside Turn Results	46
3. Rapid Starts from Neutral Pose	52
Chapter 6. Discussion	67
Is Angular Momentum Regulated during Turning and Rapid Starts?	67
Participant Independent Measures	69
Comparing the magnitude of whole-body angular momentum in rapid starts and walking	69
Comparing the magnitude of the whole-body angular momentum in the transverse plane for turning	70
Comparing Left and Right Turns - A Pilot Study on Segmental Contributions	70
Chapter 7. Conclusion	73
Appendix	75
Principal Component Analysis Background	75

Lab Specific Considerations for Ground Reference Trajectory Calculations	76
Theory of Angular Momentum Primitives	79
Bibliography	81

## List of Figures

- |   |   |    |
|---|---|----|
| 1 | The population of baby boomers is rapidly aging, which can be seen in the results of source: <a href="http://www.whitehouse.gov/omb/budget/fy2009/images/outlook-6.jpg">http://www.whitehouse.gov/omb/budget/fy2009/images/outlook-6.jpg</a>  | 16 |
| 1 | The CMP is the point the where a line parallel to the ground reaction force would have to pass through in order for the moment about the CM to be zero.[5]  | 23 |
| 1 | Outline of the turning and rapid start trials conducted at the Holodeck at CSAIL. The subject was asked to turn at a right angle and abrupt starts took place in the walking direction indicated in the figure. The orientations of each force-plate differ according to the manufacturers specification. The orientation of the lab frame was different than that of the force-plates. Due to this the location determined for the COP of the force-plate had to be moved into lab frame coordinates during post-processing. | 26 |
| 2 | A visual representation of the calculation for the CP on a force plate. Four force transducers at each corner sum individual readings, $F_1, F_2, F_3, F_4$ , to give a resultant free torque $T_z$ , and ground reaction force $F$ .(www.kwon3d.com)   | 27 |
| 3 | The location of a hypothetical location of CP and the corresponding axis in force plate coordinates.  | 28 |
| 4 | The Holodeck facility at the Computer Science and Artificial Intelligence Laboratory. The facility contains 16 IR pulse cameras recording motion at 120 hz and floor-level force-plates captures ground reaction forces at 1080 hz.   | 29 |
| 5 | A sample of the data taken from a motion capture study involving the subject 'AlGr' and the markers labelled 'C7', 'Clav', etc. with their respective 3D positions, $x, y, z$ .   | 29 |
| 6 | Flow chart of the data processing conducted to obtain resulting data (ovals) by analysis methods (blocks).  | 31 |
| 1 | This is a rendering of the morphologically accurate model [5] of the human body used to estimate the spin angular momentum about the CM. The model has 38 external degrees of freedom, or 32 internal degrees of freedom. This corresponds to 12 for the legs, 16 for the arms, and six for the rest of the body. The radii and lengths of the truncated cones are taken from physiological measurements of each participant.   | 34 |
| 2 | An outline of a foot on the ground. The medio-lateral direction corresponds to the $X$ direction and the anterior-posterior corresponds to the $Y$ direction.   | 37 |
| 1 | The whole-body angular momentum. Values are normalized by $M \cdot V \cdot H_{subject}$ . This is an average of 5 participants with 10 trials walking at a fast pace 1.5 m/s in the saggittal direction. Red dashed lines indicated a standard deviation above and below the mean of the angular momentum data in blue.   | 46 |
| 2 | The three direction for the first PC for straight walking at 1.5 m/s. The components are in order from 1 - 16 : left foot, right foot, left shin, right shin, left thigh, left hand, right  |    |

	hand, right thigh, left forearm, right forearm, left upper arm, right upper arm, lower torso, upper torso, neck, and head. Note that the contributions from each lower limb over the whole gait cycle is roughly equal. Walking is cyclic and over one gait cycle. Note that each limb makes an roughly equal contribution to total whole-body angular momentum.	47
3	Ground reference trajectories CP (green), CMP (red) and CM (blue) during walking straight. Note that the CP and CMP stays within the foot during stance on each foot. This is in agreement with previous observations of ground reference trajectories during level ground walking.	48
4	Participant-Independent Results for the first three PCs of each trial that account for more than 90% of the variance observed in data for walking straight at 1.5 <i>m/s</i> . The data explained by each PC for: (X): 85.3%, 10.3%, 2.1%; (Y): 82.8%, 9.6%, 4.4%; (Z): 88.4%, 6.2%, 4.3%.	49
5	Whole-body angular momentum averaged across 5 participants with 10 trials/participant for a Turn. This results in a total 50 trials. Each curve was normalized by the mass, velocity, and height of the <i>CM</i> through the turn, see Table 2 for values. The red-dotted lines are one standard deviation above and below the mean.	52
6	The three directions for the first PC for turning averaged for 5 participants taking 10 turns each. The components are left foot(1), right foot(2), left shin(3), right shin(4), left thigh(5), right thigh(6), left hand(7), right hand(8), left forearm(9), right forearm(10), left upper arm(11), right upper arm(12), lower torso(13), upper torso(14), neck(15), and head(16). Note that PC1 of the Z direction has segments that contribute a large unbalanced amount of angular momentum about the <i>CM</i> . The components that do this correspond to the right foot, shin and thigh.	53
7	A participant-independent comparison between the variance contributed to the first PC in both Walking (Top) and a Turn (Bottom) in the transverse plane. The right foot contributed a great amount of variance to the first PC than left foot.	54
8	Example Left Turn Trial	54
9	Ground reference trajectories CP (green), CMP (red) and CM (blue) during a turn. Note that the CP and CMP stays within the foot (the markers indicating the fifth metatarsil, the big toe and heel are in pink) during stance on each foot.	55
10	The predicted medio-lateral forces showed poor agreement with experimentally observed values. The increase in the experimental values of the medial ground reactions corresponded to the period when the turn starts after 50% turn-cycle.	57
11	Participant-Independent Results for the first three PCs of each trial that account for more than 90% of the variance observed in the data for turning. The data explained by each PC for: (X): 85.3%, 10.3%, 2.1%; (Y): 82.8%, 9.6%, 4.4%; (Z): 88.4%, 6.2%, 4.3%.	58
12	The mean values over all participants and trials of the normalized tuning coefficients associated with a one-step turn to the left. From the top to the bottom are the (X), (Y) and (Z) directions, respectively. These normalized tuning coefficients were obtained using Eqn. 13 of Chapter 4.	59
13	Example Rapid Start	60
14	Whole-body angular momentum averaged across 5 subjects with 10 trials each. This results in a total 50 trials. Each curve was normalized by the mass, velocity, and height of the <i>CM</i> through the turn, see Table 5 for values. The red-dotted lines are one standard deviation above and below the mean.	61



- 15 The three direction for the first PC for an abrupt start. Red bars indicate one standard deviation above and below the mean. The components are left foot(1), right foot(2), left shin(3), right shin(4), left thigh(5), right thigh(6), left hand(7), right hand(8), left forearm(9), right forearm(10), left upper arm(11), right upper arm(12), lower torso(13), upper torso(14), neck(15), and head(16). 62
- 16 Ground reference points tracking the CM during an abrupt start. The CP, CM, CMP are green, blue, and red respectively. The markers indicate the location of the heel, metatarsil five, and big toe marker. 63
- 17 Participant-Independent Results for the first PCs of each trial that account for more than 90% of the variance observed in the data for a rapid start. The data explained by each PC for: (X): 73%, 16.6%, 7.6%; (Y): 52%, 23.1%, 10.4%, 7.1%; (Z): 69.9%, 16.7%, 6.6%. 64
- 18 Single Subject Data: The anterior-posterior direction shows good agreement between the predicted and observed data. The medio-lateral direction shows relatively poor agreement between the predicted and experimental data. 65
- 19 The mean values over all participants and trials of the normalized tuning coefficients associated with a rapid start. From the top to the bottom are the (X), (Y) and (Z) directions, respectively. These normalized tuning coefficients were obtained using Eqn. 13 of Chapter 4. 66
- 1 A close-up of the CMP (red) and CP (green) on the first step of a rapid start. The CMP is outside of the approximate region of foot support during stance. This suggests that the moments acting on the CM might have been quite large. Large enough to push the CM outside of foot support. 68
- 2 The results of PC analysis on data obtained for a right handed turn. Note that the Z direction shows a similar and opposite contribution from the left and right lower limbs. 71
- 1 A depiction of the transfer of support during the initial stages of the gait cycle. 77
- 2 The Normal Gait Cycle. Figure taken from NEJM, 1990. 77



## List of Tables

1	Data Explained in walking for 10 Trials Per Subject over one gait cycle	46
2	Data Explained for Turning for 10 Trials Per Subject for one whole Gait Cycle	56
3	Body mass $M_{subject}$ , $CM$ height $H_{subject}$ and average speed through the turn, $V_{subject}$ for each study participant	56
4	Data Explained in Rapid Starts for 10 Trials Per Subject	60
5	Body mass $M_{subject}$ , $CM$ height $H_{subject}$ and average speed through the period of rapid starting (including stance prior to start) $V_{subject}$ for each study participant	61



## CHAPTER 1

# Introduction

### 1. Outline of Thesis

The study of the human body has long influenced technology by providing constraints on the design of devices that enable us to move faster, explore our environment, and rehabilitate from accidents. The study of biomechanics has influenced the design of prosthetics and more recently the study of human motion is having a similar influence on humanoid robotics. Humanoids (humanoid robots) are being developed to act as personal assistants and robotic prostheses are being created that give an amputee the needed power to move swiftly about the world with significantly reduced metabolic effort when compared with their un-powered prosthetic.

What makes the above advances possible are efficient controllers that utilize known mechanics. In the case of wearable prostheses one important goal is biomimetics. That is to accurately mimic a normal person's gait through a controller in a robotic prosthetic. In the case of humanoid robotics the goal would be to develop efficient and flexible controllers that allow robots to express itself dexterously.

In the past, bipedal robotic machines have used a Zero Moment Point (ZMP) strategy to design joint trajectories to produce stable level ground walking. The ZMP was discovered by studying the movement of the center of mass (CM) above the ground support base many years ago [4]. Though some multi-link robots are used with other control strategies for path planning, in addition to ZMP control, the development of pre-computed trajectories largely ignored issues of robustness to disturbances. This is evident in humanoids that use high gain ZMP controllers to play back pre-computed trajectories where stability is guaranteed as long as the CM stays above the ground support base. However, these controllers immediately failed when a disturbance pushed it out this region, which can potentially damage the robot or any near-by humans.

This forced us to confront a very difficult challenge; to build machines that are robust, but are able to recover and adapt quickly to an environment with humans and other moving objects

everywhere. One way to approach this problem is to understand the ways that humans accomplish things like turning and abrupt starts. By understanding the biomechanics of these transient motions we motivate the development of whole-body angular momentum controllers for a Humanoids or lower limb prostheses.

This last goal, mentioned in the above paragraph, is the eventual drive of this biomechanics study of transients. Motivating controls from biological observations of angular momentum is an indirect way to approach humanoid control. However, many times in robotics mechanical intuition is used to develop controls as a substitute for actual data. While this has been successful in many applications, direct data can back up that intuition with biological observations.

The development of the experimental protocol and the background literature on the topic of transients in biomechanics is reviewed. Following this, a review of how what was researched is novel in light of this set of background and how we proposed to improve upon previous work. Then a general analytical technique was proposed for motion capture to obtain angular momentum magnitude and distribution. In addition, ground reaction force data were collected; I derived ground reference trajectories and discussed their implications to center of mass stability by looking at the *CMP*.

Motivated by the recent work of Herr and Popovic [6] we explored the following hypotheses applied to turning and rapid starts. Given the results of a pilot study [37] on turning and pilot data from rapid starts that whole-body angular momentum remained relatively small through these transients, we hypothesized that horizontal ground reaction forces and the Center of Pressure (CP) trajectory in each transient can be explained predominantly through an analysis that assumed a zero-moment about the body's center of mass (CM). To test this we derived the theoretical horizontal ground reaction force and where the *CP* location would be if the horizontal moments about the CM were zero. This was tested using a 16-segment human model and gait-data obtained from 10 study participants.

Also, I examined segmental contributions to the whole-body angular momentum for rapid starts and turning. Despite the fact that segments produce substantial, and sometimes unequal amounts of angular momentum about the CM, the whole-body angular momentum remains small. This indicates a large amount of segment-to-segment angular momentum is being cancelled. Unique to turning is the use of a limb to produce a moment about the CM for the completion of the turn,

also, rapid starts involve the production of horizontal moments about the CM to lunge the body forward. How these unbalanced moments effect segmental cancellations are considered.

The use Principal Component Analysis (PCA) was applied to segment angular momentum time-series data as a way to find those parts of the body whose statistical variance was high. Therefore important during the proposed transient motions of rapid starts and turning in a statistical sense.

## 2. Societal Motivation and Demand

As mentioned in the previous section, we looked to enhance the ability of humanoid robots to move comfortably in an unstructured human environment. Why is this? While a robotic assistant could certainly be seen as useful to a busy executive is there a direct need that can be satisfied by this system? Two places in the developed world that are going to see a future increase in the number of elderly and in-home care patients are Japan and North America, see Fig. 1. According to the US Administration on Aging, approximately 37.3 million of persons in the US are over the age of 65 as of 2005. A significant percentage of these people suffered from some sort of disability that impaired their mobility. In the 65-75 age group, approximately 50% has some disability, not necessarily mobility related. However, of these people with disabilities approximately 49% had arthritis related disabilities, and almost 18% had orthopedic related difficulties.

These impairments have a very real impact on the daily lives of this rapidly growing population. Over the next 40 years the trend of increasing mobility impairment among elderly people is unlikely to decrease. Humanoid robotics and intelligent prosthetics, will very likely provide the most effective solution to this encroaching problem. They will provide the care needed in the homes of the elderly; robotic prosthetics will allow people to regain much of their fluidity of movement. Much like what their bodies were accustomed to in their youth.

Humanoids have some unique features that separate them from other quadruped or wheeled robots. Humanoid robots have a small support base that is naturally constrained by the location of the feet relative to the ground projection of the CM. This has the advantage that it can move through a small space, but the robot's CM is placed high relative to the feet making the stability of the robot highly sensitive to disturbances about the CM. A feature normally not encountered on quadrupedal robots and wheeled robots that typically have lower CM. When the CM is outside the ground support polygon this usually indicates that the robot has fallen over. If this were an

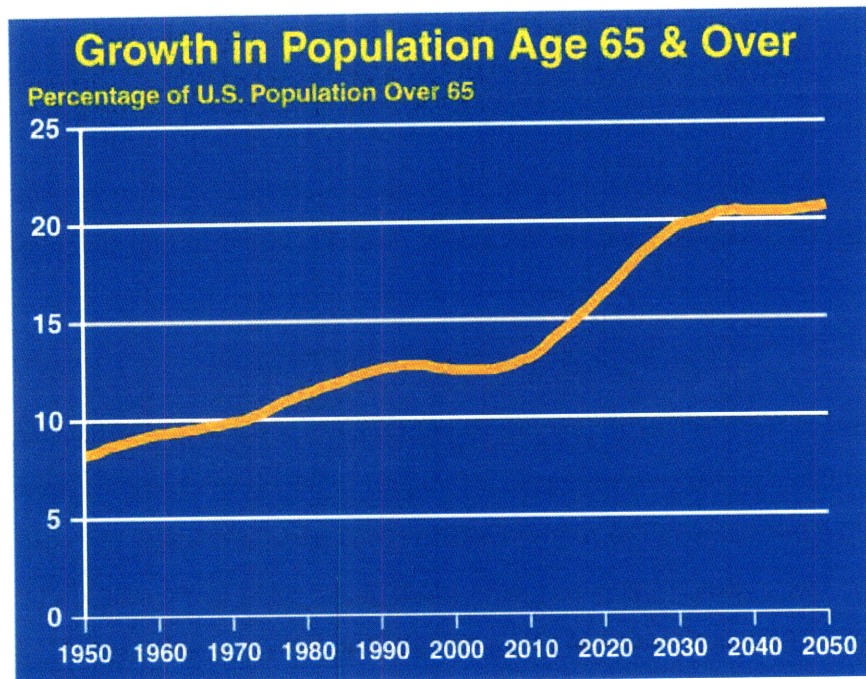


Figure 1: The population of baby boomers is rapidly aging, which can be seen in the results of source: <http://www.whitehouse.gov/omb/budget/fy2009/images/outlook-6.jpg>

exoskeleton, this would indicate the person fell over and is now on the ground. This means any control should place a high priority on this constraint always remaining satisfied. The difficulty is to maintain this constraint while not making the motions unnecessarily rigid. Such rigidity can make an exoskeleton unusable in a practical setting.

### 3. Problem Statement

The observation of humans during particular tasks has led to insights into the how the body maintains balance during steady-state walking. Can the same method be applied to the study of transients in human walking? More specifically, the following questions will be addressed both transients;

- We hypothesize that whole-body angular momentum remains small about the CM for the duration of each transient. Therefore, an analysis of the horizontal ground reaction forces can be largely explained through a zero-moment strategy.



- Further, we hypothesize that due to the small whole-body angular momentum about the CM, and large segmental angular momentum, that there must be large segment-segment cancellation.

Specifically, for turning we propose that;

- Motivated by initial pilot study finding that the swing leg during and inside turn produce the most angular momentum about the CM during a turn.

and for a rapid start that;

- That the upper torso produces a non-negligible angular momentum about the CM that is balanced by the initial swing-leg during a rapid start.

The next chapter will cover the relevant background for ground reference trajectories and modeling with an anthropomorphically realistic model.



## CHAPTER 2

# Background

### 1. Previous Work

The study of human biomechanics is very old going back several hundred years. As early as the beginning of the 20<sup>th</sup> century Elftman [3] was able to conduct a motion capture study with a kind of chemical force-plate. From this he defined a "position for force" for both static and dynamic cases. After this Vukobratovic and Juricic [4] expanded Elftman's point to be applicable for legged machine control.

In terms of angular momentum, there has been much work done on non-walking tasks such as sit-to-stand maneuvers [24], running [25][26][27][28] and a variety of sporting activities [32][29][30][31][33][34]. These studies have look mainly at the contributions of angular momentum for different sports.

Xu and Wang estimated angular momentum contributions from the lower limbs for altering direction during walking [12]. In 2000 [35] studied angular momentum in older populations, a group prone to falling, to understand deficiencies in balance. They found the angular momentum characteristics of "frequent fallers" and "non-fallers" were similar. However, the ankle and knee torques of "frequent fallers" were smaller than those of "non-fallers". This, they suggested, was the reason for their frequent falls. Their inability to control appropriate torques led to frequent falls. However, they were restricted by the smaller numbers of subjects they used during their analysis (three "non-fallers" and two "frequent-fallers").

Herr and Popovic were able to show that the body tightly regulated angular momentum about the CM during every phase of the gait cycle [6]. Herr [6] quantifies angular momentum contributions and cancellations for a 16 segment model of the human body. They obtained principal components describing the whole-body angular momentum in a latent space where contributions to each of the components, in each direction, indicated the source of whole-body angular momentum cancellation.

However, they restricted attention to normal level ground walking and an exaggerated walking gait. This study does not include angular momentum in more complex behaviors.

Transient behavior biomechanics literature will often use the term "anticipatory postural adjustments" to refer to changes in posture prior to the voluntary initiation of a movement. In the case of turning and rapid starts these anticipatory adjustments can be viewed as those changes in balance that contribute to the successful completion of a turn or start. In a study by [12], researchers found "participants leaned backward and sideward on the prior step in anticipation of the turn. Those findings indicate that the motor system uses central control mechanisms to predict the required anticipatory adjustments and organizes the body configuration on the basis of the movement goal".

Orendurff [13] noted that at slow-speeds turning on the inside foot resulted in a non-uniform center of mass trajectory. However, the most profound difference was observed in the mediolateral ground reaction force impulse. In level ground walking the impulses tend to push the body towards the opposite foot that will soon be assisting in double support (contralateral limb). In turning, the impulses for different types of turns shifted the body towards the ipsilateral and contralateral limbs, respectively. Further studies include the neuroscience of turning, [20], and what strategies the muscles are used to complete a turn. These studies indicate a large amount of prepared postural control is exercised during the initiation of the turn. In a study by Frasso, Zago, and Lacquaniti [38] subjects were asked to walk with their torso upright, then with their knees slightly bent, then again with their torsos bent and their knees bent. Principal Component Analysis (PCA) was applied to the elevation angles over the gait cycle. From these data they observed a similar control of limb segment rotation in both quadrupedal locomotion and bipedal locomotion. In addition, their observations concerning the laws of inter-segmental coordination might emerge from the coupling neural oscillators and mechanical oscillators. That hypothesis that the law of coordinative control results from minimal active tuning of passive inertial and viscoelastic coupling among limb segments suggests that walking, among all animals, evolved using minimum-energy as a criteria.

This author has not encountered other work separate from the above that has approached the use of an anthropomorphic model, PCA and a zero-moment analysis as a way to understand the biomechanics of turning and rapid starts.

In robotics, angular momentum has been used to control bipedal robotic walking; below are definitions derived from that literature.

## 2. Ground Reference Trajectories

In the literature on biomechanics and control there are several different ground reference trajectories used to monitor the stability of a legged system. By monitoring the relationship between the different ground reference trajectories it was possible to gain insight into the dynamic behavior of a bipedal mammal, namely a human. Not only do the trajectories indicate the degree of stability in a system, but they provide an important criteria and constraints in the development of whole-body balance control schemes.

The important ground reference trajectories in this thesis are the Center of Pressure (CP), Zero Moment Point (ZMP) and the Center Moment Pivot (CMP)[5].

### 2.0.1. ZMP - Zero Moment Point.

DEFINITION 1 (COP). *The location where all the resultant of all ground reaction forces act.*

DEFINITION 2 (ZMP). *The point on the ground surface about which the horizontal component of the moment of the ground reaction force is zero.*

In practice this means the ZMP, denoted  $r_{ZMP}$ , is the point on the ground about which the moment's horizontal component of the ground reaction force is zero[4][15]. More specifically, let

$$(1) \quad \vec{\tau}_{G.R.}(\vec{r}_{ZMP})|_{horizontal} = 0,$$

where  $\vec{\tau}_{G.R.}$  is the moment about  $r_{ZMP}$ , be the horizontal component of the net moment about  $r_{ZMP}$ . Therefore, by this definition the whole-body torque at  $r_{ZMP}$  exerted on the body was parallel to gravity. This leads to another property of the point,  $r_{ZMP}$  that is

$$\vec{\tau}_{inertia+gravity}(\vec{r}_{ZMP})|_{horizontal} = 0.$$

This alternate definition of  $r_{ZMP}$  treats the ZMP as the location on the ground where the net moment due to gravitational and inertial forces has no component along the horizontal axis [4][16][17]. These two definitions for the ZMP are both equivalent as was shown in [7]. Following

the same derivation given in [5], note that if there are no external forces except the ground reaction forces

$$\vec{\tau}(\vec{r}_{ZMP})|_{horizontal} = [(\vec{r}_{CM} - \vec{r}_{ZMP}) \times M\vec{g}]|_{horizontal}.$$

In the case of level ground it can be shown that the  $COP = ZMP$ . This an important assumption that we will use throughout this work. The following is the proof presented in [5]:

For a body at rest on a horizontal plane the  $CP$  is defined as,

$$(2) \quad \vec{r}_{CP} = \frac{\int_{gsb} \vec{r} p(\vec{r}) da}{\int_{gsb} p(\vec{r}) da} = \frac{\vec{\tau}_{G.R.}(0)|_{horizontal}}{F_Z} \times \frac{\vec{g}}{g},$$

where the integral is over the ground support based (gsb) defined by the biped and  $da$  is a sufficiently small area of the gsb at  $\vec{r}$ ,  $p(\vec{r})$  is the pressure at point  $\vec{r}$ ,  $F_Z$  is the vertical component of the ground reaction force, and  $g$  is gravity. The second equality results from the assumption that  $p(\vec{r}) da = dF_Z$  and  $\vec{r} \cdot \vec{g} = 0$ .

Therefore, the moment exerted on the body from the ground about the origin of the lab frame on the ground is:

$$(3) \quad \vec{\tau}_{G.R.}(0)|_{horizontal} = \int_{gsb} (\vec{r} \times d\vec{F}_{G.R.})|_{horizontal}$$

$$(4) \quad = \int_{gsb} (\vec{r} \times \frac{\vec{g}}{g}) p(\vec{r}) da$$

$$(5) \quad = \frac{\vec{g}}{g} \times \int_{gsb} \vec{r} p(\vec{r}) da.$$

Then assuming the conditions given for Eqn. 2, note that  $\vec{\tau}_{G.R.}(\vec{r})|_{horizontal} = \vec{\tau}_{G.R.}(0)|_{horizontal} + F_Z \vec{r}_{CP} \times \frac{\vec{g}}{g} = 0$ .

Then by re-writing 1, we derive another relation,

$$\vec{\tau}(\vec{r}_{ZMP})|_{horizontal} = \int_{gsb} [(\vec{r} - \vec{r}_{ZMP}) \times d\vec{F}]|_{horizontal} = - \int_{gsb} [(\vec{r} - \vec{r}_{ZMP}) \times \frac{\vec{g}}{g}] dF_Z = 0,$$

that becomes,

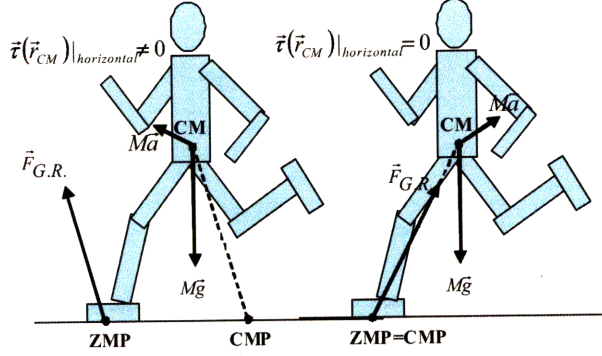


Figure 1: The CMP is the point the where a line parallel to the ground reaction force would have to pass through in order for the moment about the CM to be zero.[5]

$$\vec{\tau}(\vec{r}_{ZMP})|_{horizontal} = - \int_{gsb} (\vec{r} \times \frac{\vec{g}}{g}) dF_z + \frac{\int_{gsb} \vec{r} dF_z}{\int_{gsb} dF_z} \times \frac{\vec{g}g}{\int_{gsb} dF_z} = 0.$$

proving that for horizontal contact planes the *ZMP* and *CP* coincide.

DEFINITION 3 (CMP). From Popovic and Herr [5] the *CMP* is defined as the point where a line parallel to the ground reaction force, passing through the *CM* in the lab frame, intersects with the external contact surface, Fig. 1

The use of this definition in biomechanics literature was to assess how the moments are acting about the *CM*. When there are no moments acting about the *CM* then the condition  $CMP = ZMP$  is satisfied and the ground reference trajectories are at the same location on the ground. However, if the horizontal moment about the *CM* is non-zero then  $CMP \neq ZMP$ . These properties follow from the following definitions of the *CMP*; the mathematical definition for the point is given by,

$$[(\vec{r}_{CMP} - \vec{r}_{CM}) \times \vec{F}_{G.R.}]|_{hor} = 0,$$

with  $z_{CMP} = 0$ , and  $\vec{r}_{CMP}$  is the position of the *CMP* on the ground,  $\vec{r}_{CM}$  is the position of the *CM* on the ground, where  $\vec{F}_{G.R.}$  is the vector of ground reaction forces. Then by letting  $\vec{r}_{CMP} = (x_{CMP}, y_{CMP}, 0)$ ,  $\vec{r}_{CM} = (x_{CM}, y_{CM}, z_{CM})$ ,  $\vec{F}_{G.R.} = (F_{G.R.X}, F_{G.R.Y.})$  and taking the cross product yields,

$$x_{CMP} = x_{CM} - \frac{F_{G.R.X.}}{F_{G.R.Z.}} z_{CM},$$

and

$$y_{CMP} = y_{CM} - \frac{F_{G.R.Y.}}{F_{G.R.Z.}} z_{CM}.$$

These definitions are useful for their ease of use in calculations with data collected from analog strain-gauge force-plates and motion capture data. Also, note that when the horizontal ground reaction forces are zero, the CMP coincides with the ZMP.



## CHAPTER 3

# Experimental Methods

### 1. Human Subject Experiments

We obtained kinematic and force-plate data for five subjects during a left inside turn and rapid starting. For each human motion experiment participants gave their informed consent to participate in this study. Each subject was free of musculoskeletal and orthopedic problems by self-report.

Subjects were brought to a motion capture facility at the Computer Science and Artificial Intelligence Laboratory (<http://csail.mit.edu>) for trials. Force and kinematic data were collected with an AMTI force platform and a 16 camera motion capture system VICON 810i (Oxford Metrics, Oxford, UK), respectively. A total of 41 markers were placed on each subject according the VICON golem model specifications. Each subject completed a 90° left turn by pivoting for the turn on the left foot, so that the recovery foot was the right foot. The subjects walked at 1.5 m/s entering into the turn and wore bare-feet during the study. Fig. 1 shows the direction participants followed during this study.

The starting study was conducted with subjects in bare-feet. The subjects stood motionless on a force-plate, for between 1-3 seconds, before being instructed to accelerate as fast as possible at randomly selected times within that range. This simulates a rapid full-speed acceleration. Each subject's acceleration speed was therefore self-selected to be as fast as possible.

**1.1. Comparison of Turning Protocol with previous literature.** In our study we used one type of turn. In [20] this was referred to as the 'spin turn' and in this thesis is referred to as the inside turn because it takes place on the ball of the foot and on the same side of the body as the turn. We did not study the so-called 'step turn' which takes place on the outside foot of the turn. One further difference between our protocol and [20] was how the turn took place.

Our protocol asks subjects to perform a practiced inside turn where-as a turn in [20] resulted in the subjects returning to their original location. This means they are performing an 'about

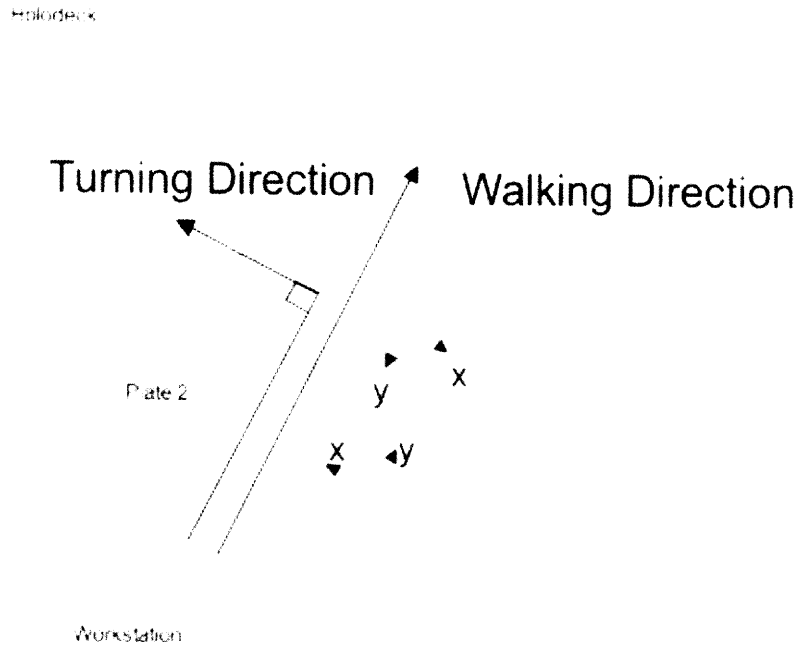


Figure 1: Outline of the turning and rapid start trials conducted at the Holodeck at CSAIL. The subject was asked to turn at a right angle and abrupt starts took place in the walking direction indicated in the figure. The orientations of each force-plate differ according to the manufacturers specification. The orientation of the lab frame was different than that of the force-plates. Due to this the location determined for the COP of the force-plate had to be moved into lab frame coordinates during post-processing.

face’ where-as we are assuming the common situation of a subject taking a turn at  $90^\circ$  and then continuing to walk straight.

Other researchers used different protocols; for example [?], only specified the degree of the turn to be between 0, 45, or  $90^\circ$  and the speed to be  $1.5\text{ m/s}$  they allowed the direction and type of turn, spin or step, to be arbitrary.

Again, in our case the desire is to see how the people accomplish a practiced inside turn. We controlled for the angle, direction and speed leaving less room for variability between subjects. Also, in-order for the turn to be comparable to walking straight or a rapid start we designated the turn to take place in three steps; the first step on the force plate, double support on both plates, and finally the last step of the turn and return to level ground straight walking.

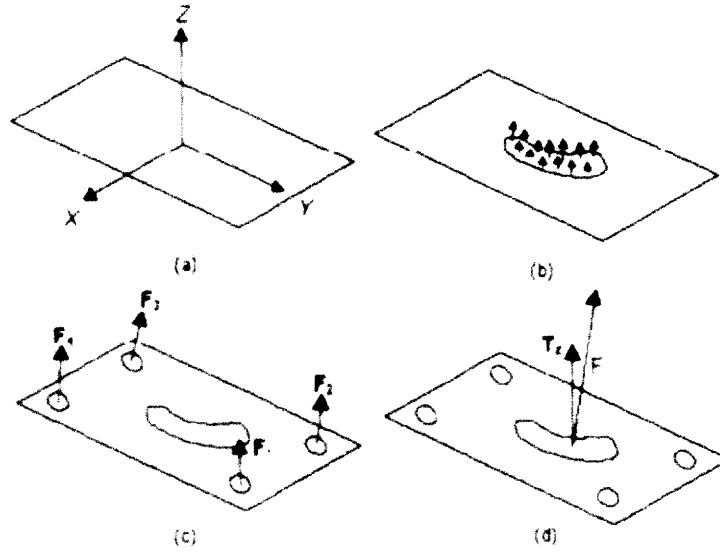


Figure 2: A visual representation of the calculation for the CP on a force plate. Four force transducers at each corner sum individual readings,  $F_1, F_2, F_3, F_4$ , to give a resultant free torque  $T_z$ , and ground reaction force  $F$ .(www.kwon3d.com)

## 2. Force Plates Details

Two force-plates, model BP600900 - 2000 from Advanced Mechanical Technologies, Inc. (AMTI ©), were used to collect ground reaction forces during each of the tasks. Each plate measured the location of the center of pressure and the ground reaction force with respect to the local, force-plate coordinate system.

The location of the CP was calculated using a script developed by Vicon Motion Systems. In general the physical center of the force plate does not correspond exactly to the center determined by the force transducers at the corners of the force plates. However, this can be accounted for in the specifications of the manufacturer of the plates. Fig. 3 shows the location of force applied to the force plate and the associated CP as well as the origin of the force plate coordinate system.

To obtain the location of the CP in force plate coordinates the following transformations are applied;

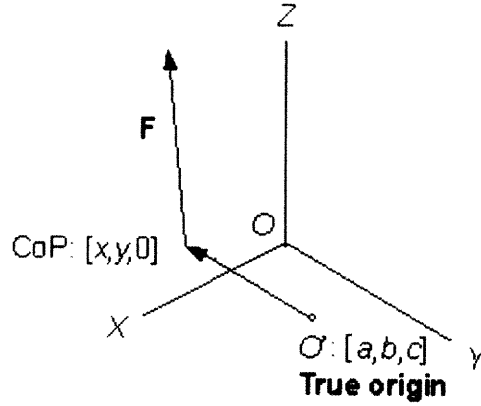


Figure 3: The location of a hypothetical location of CP and the corresponding axis in force plate coordinates.

$$\begin{pmatrix} M_x \\ M_y \\ M_z \end{pmatrix} = \begin{pmatrix} 0 & c & y-b \\ -c & 0 & -(x-a) \\ -(y-b) & x-a & 0 \end{pmatrix} \begin{pmatrix} F_x \\ F_y \\ F_z \end{pmatrix} + \begin{pmatrix} 0 \\ 0 \\ T_z \end{pmatrix} = \begin{pmatrix} (y-b)F_z + cF_y \\ -cF_x - (x-a)F_z \\ (x-a)F_y - (y-b)F_x + T_z \end{pmatrix}$$

Therefore, the position on the plate of the *CP* is,

$$(6) \quad x = -\frac{M_y + cF_x}{F_z} + a$$

$$(7) \quad y = \frac{M_x - cF_y}{F_z} + b$$

$$(8) \quad T_z = M_z - (x-a)F_y + (y-b)F_x.$$

Therefore, the position of the CP can be computed from the moment caused by the ground reaction force about the true origin,  $M_x$ ,  $M_y$  and  $M_z$ , the ground reaction force,  $F_x$ ,  $F_y$  and  $F_z$ , and the location of the true origin,  $a$ ,  $b$  and  $c$ .  $M_x$ ,  $M_y$ ,  $M_z$ ,  $F_x$ ,  $F_y$  and  $F_z$  can be directly measured from the 6 channels of the AMTI plates while the position of the true origin can be found in the calibration data sheet.



Figure 4: The Holodeck facility at the Computer Science and Artificial Intelligence Laboratory. The facility contains 16 IR pulse cameras recording motion at 120 hz and floor-level force-plates captures ground reaction forces at 1080 hz.

Time	AIGr:C7:X	AIGr:C7:Y	AIGr:C7:Z	AIGr:CLAV:X	AIGr:CLAV:Y	AIGr:CLAV:Z	AIGr:COP	FP1	AIGr:COP	FP1
0	289.23	2004.4	1387.4	298.59	1876.8	1329.2	300		450	
0.0083	289.05	2004.3	1387.5	298.72	1876.7	1329.3	300		450	
0.0167	289.16	2004.2	1387.5	298.79	1876.7	1329.3	300		450	
0.025	289.28	2004.2	1387.6	298.74	1876.8	1329.3	300		450	
0.0333	289.38	2004.2	1387.5	299.25	1876.9	1329.1	300		450	
0.0417	289.61	2004.3	1387.5	300.34	1877	1328.8	300		450	
0.05	289.69	2004.4	1387.6	300.35	1876.9	1328.9	300		450	
0.0583	289.59	2004.4	1387.5	299.32	1876.8	1329.1	300		450	
0.0667	289.6	2004.4	1387.4	298.87	1876.8	1329.1	300		450	
0.075	289.69	2004.4	1387.3	298.98	1876.7	1329.1	300		450	
0.0833	289.71	2004.4	1387.3	299.01	1876.8	1329.1	300		450	
0.0917	289.7	2004.4	1387.4	298.94	1876.8	1329.1	300		450	
0.1	289.71	2004.5	1387.4	298.95	1876.7	1329.1	300		450	
0.1083	289.82	2004.5	1387.4	299.49	1876.8	1329.1	300		450	
0.1167	290.01	2004.4	1387.4	300.5	1876.9	1328.9	300		450	
0.125	290.09	2004.3	1387.4	301.05	1876.9	1328.8	300		450	
0.1333	290.12	2004.3	1387.4	301.08	1876.9	1328.7	300		450	
0.1417	290.13	2004.3	1387.4	300.55	1876.9	1328.8	300		450	
0.15	290.03	2004.3	1387.3	299.52	1876.9	1329	300		450	
0.1583	289.99	2004.2	1387.3	299.1	1876.8	1329	300		450	

Figure 5: A sample of the data taken from a motion capture study involving the subject 'AIGr' and the markers labelled 'C7', 'Clav', etc. with their respective 3D positions,  $x, y, z$ .

### 3. Motion Capture Details

Motion capture data was collected for each subject. Passive reflective markers were placed on each subject according the golem kinematics model provided by Vicon Motion Capture systems©. Markers are placed on each of the joints and along the arm and leg segments, as well as, on the head, along the spine, and on the torso. The system is able to capture motion data 120 hz with an accuracy of  $\approx 1mm$ . The data produced by the system comes in the form of text file that contains a matrix of columns representing the  $x, y, z$  position of each marker from the model, Fig. 5.

#### 4. Data Analysis Pipeline

In this work, the kinematic and analog data were collected and analyzed, Fig. 6 using a Vicon system that reported the location of individual markers as a location, in millimeters, in the three dimensional lab-frame. In addition, analog data are reported in a similar fashion to those of the markers. Each three axis force-plate reports  $F_x, F_y, F_z, M_x, M_y,$  and  $M_z$  in addition to the  $COP$  as was explained in the Experimental Methods section of this thesis. These data were synched and down-sampled in hardware to correspond with kinematic sampling rate. These kinematic data were then used to calculate the  $CM$  location from the human body model described in this chapter. This allowed for the calculation of the  $CMP$  trajectory by combining analog and kinematic data. From the human body model, and using kinematic data, I directly calculated the segmental angular momentum about the  $CM$ . Then using the time-series data for the angular momentum I used PCA to reduce dimensionality of the high-degree of freedom human body model.

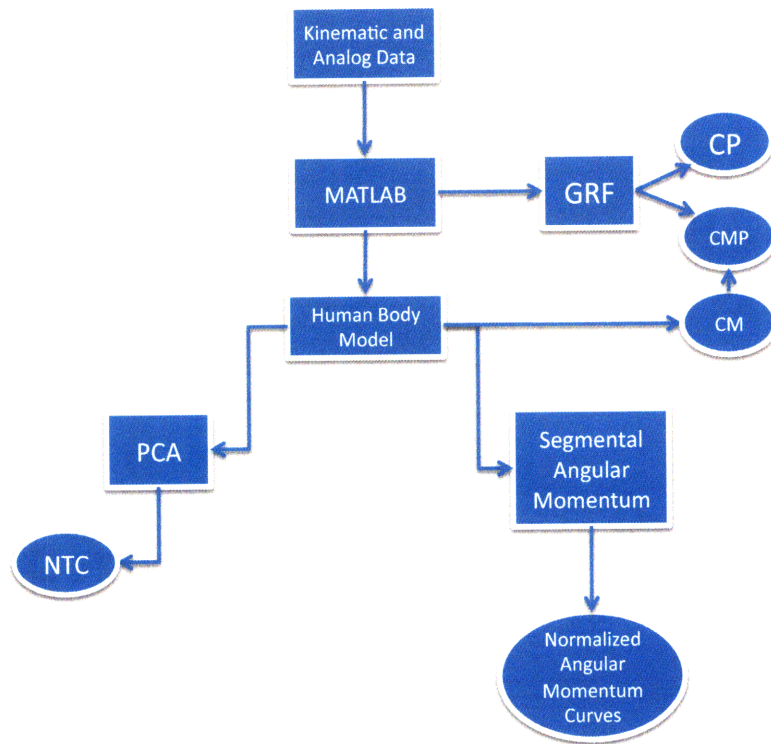


Figure 6: Flow chart of the data processing conducted to obtain resulting data (ovals) by analysis methods (blocks).





## CHAPTER 4

# Analytical Methods

### 1. Human Model

In our work we cannot assess the amount of angular momentum about the CM without an appropriate model for the human body. For this reason we developed a morphologically realistic model that served as a representation of the different segment lengths and thicknesses normally encountered in different people. This was done by taking participant measurements and using weight distributions[22] to predict the location of the CM and whole-body angular momentum about the CM by the movement of truncated cones, cylinders and sphere.

To estimate the location of the CM, for calculation of the *CMP* and angular momentum contribution of each limb relative to the body's total center of mass a *truncated cone model* [5] was used. The model treats limb segments as truncated cones to account for the differences in mass distribution about a specific limb, Fig.1.<sup>1</sup>

The model [6][5] was comprised of 16 rigid body segments: feet, tibias, femurs, hands, forearms, arms, pelvis-abdomen, chest, neck and head. The segments represented the tibia, femur, forearms, and arms as truncated cones. The trunk was broken into lower (pelvis-abdomen) and upper (chest) segments (modeled as ellipsoidal slabs), and the head was approximated as a sphere of a constant radius.

In order to obtain realistic data for a participant we used their 21 body-length measurements:

- (1) foot and hand length width and thickness;
- (2) shanks, thighs, forearms, and upper arm lengths including their proximal and distal base radii;
- (3) thorax and pelvis-abdomen heights, widths, and thicknesses;
- (4) radius of the head, where the neck radius is half of the head radius.

---

<sup>1</sup>Note also the coordinate system was the same as the lab frame coordinate system. It was not connected to the body of the subject.

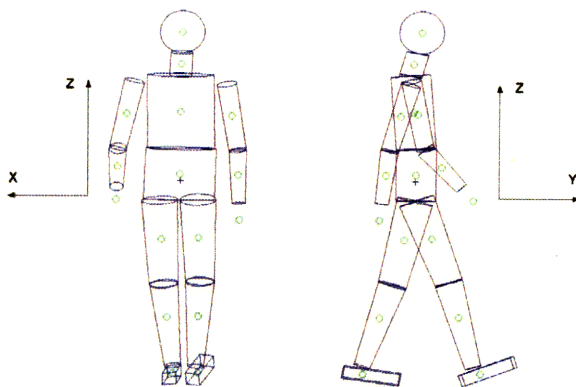


Figure 1: This is a rendering of the morphologically accurate model [5] of the human body used to estimate the spin angular momentum about the CM. The model has 38 external degrees of freedom, or 32 internal degrees of freedom. This corresponds to 12 for the legs, 16 for the arms, and six for the rest of the body. The radii and lengths of the truncated cones are taken from physiological measurements of each participant.

The model was designed so that the relative mass density was in reasonable agreement with morphological data from literature [22].

As mentioned above, the anthropomorphically realistic model uses a 16 component vector corresponding to the relative mass distribution,  $M_R$ , of the human body model segments. It is important to be aware that the mass distributions represented in the model by this vector will change the observed angular momentum. For example, by using a truncated cone model of the human body the distribution of mass cannot be directly translated from those physiological values reported by [22] from cadaver studies.

To match our human model's mass distributions with those observed in [22] we wrote the vector,  $M_R$  as a single parameter  $\alpha$  such that,

$$(9) \quad M_R(\alpha) = \frac{(M_R^{Exp} + \alpha \bar{V}_R)}{1 + \alpha},$$

where  $V_R$  is a 16 component vector of relative volumes computed directly from the truncated cone model. <sup>2</sup>

The relative volumes were computed as the ratio of the segment's volume over the total body volume. That is, if  $V^i$  is the  $i$ -th segment's volume, then the relative volume of the  $i$ -th segment

<sup>2</sup>Based on observations made of a human foot's articulated bone structure, the mass of the forefoot was estimated to be roughly 20% of the total footmass.

is  $V_R^i = V^i/V$ , where  $V$  is the total body volume. Using , in addition to, the total body mass and segments masses the 16 component vector density can be written as  $\bar{D}^i(\alpha) = M_{subject}M_R^i(\alpha)/V^i$ , where  $M_{subject}$  is the total body mass and  $V^i$  is the volume of the  $i$ -th segment. The optimal setting of  $\alpha$ , that is  $\alpha = \alpha_{\min}$  that is found by the following optimization:

$$\begin{aligned} \min |\bar{D}(\alpha) - \bar{D}^{Exp}| &= \min \sqrt{\sum_i [D^i(\alpha) - D^{Exp,i}]^2} \\ \Rightarrow \alpha_{\min} \Rightarrow \vec{M}_R &= \frac{\vec{M}_R^{Exp} + \alpha_{\min} \vec{V}_R}{1 + \alpha_{\min}}. \end{aligned} \quad 3$$

The moments and angular momentum of the model are estimated using the methods detailed in [6]. The *whole-body center of mass* is given by,

$$(10) \quad \vec{r}_{CM} = \sum_{i=1}^{16} M_R^i \vec{r}_{CM}^i,$$

where  $M_R^i$  is the relative mass of the  $i$ -th body segment and  $\vec{r}_{CM}^i$  is the CM location of the  $i$ -th body segment relative to the lab frame.

**1.1. Center of mass error.** In terms of the error associated with the CM, Herr and Popovic [6] collected kinematic data from the aerial phase of running and then, using Eqn 10, they estimated the body’s aerial phase CM trajectory. They found good agreement between the estimated CM trajectory from the Human Body model and the ballistic trajectory with  $R^2 = 0.99$ .<sup>4</sup> They noted that, during the aerial phase, the maximal distance error between these trajectories was less than 2 mm. As a further check they collected kinetic and kinematic data while a participant stood motionless in a static pose on a force-plate. The projection of the CM on the ground, as obtained from the model, was compared with the values obtained directly from the force-plate. The force-plate acted as ground truth data and the separation distance between the two points was  $\approx 3mm$ . Then they repeated this test for a different static pose; one foot was retracted to the rear and one was protracted. This position is similar to a position taken by a person in the double-support phase of walking. The error was observed to be small in this case as well, at  $\approx 3mm$ .

<sup>3</sup>In this work  $\alpha_{\min} = \frac{1}{2}$ .

<sup>4</sup>Here  $R^2 = 1 - \frac{\sum_{i=1}^{N_{trial}} \sum_{j=1}^{N_{percent}} (F_{Exp}^{ij} - F_{Mod}^{ij})^2}{\sum_{i=1}^{N_{trial}} \sum_{j=1}^{N_{percent}} (F_{Exp}^{ij} - F_{Exp}^{ij})^2}$ , where  $F_{Exp}^{ij}$  and  $F_{Mod}^{ij}$  are the forces taken at the  $j$ -th percentage gait cycle of the  $i$ -th trial from the experimental data and model-predicted data, respectively. For further details on how it was computed see [6].

**1.2. Whole-body angular momentum.** The whole-body angular momentum and moment are calculated using kinematic gait data and the human body model. The angular momentum,  $\vec{L}$ , is calculated as the sum of individual segment angular momenta about the body's center of mass (CM),

$$(11) \quad \vec{L} = \sum_{i=1}^{16} (\vec{r}_{CM}^i - \vec{r}_{CM}) \times m_i (\vec{v}^i - \vec{v}_{CM} + \vec{I}^i \vec{\omega}^i).$$

Where the first term in the cross product is the angular momentum as a result of the  $i$ -th segment's movement relative to the CM movement.

**1.3. Normalization of angular momentum curves.** Note that  $L$ , determined in Eqn. 11 has a different magnitude for each subject. In order to reduce the variance in the angular momentum there is a normalization constant that can be applied that depends on the velocity, mass, and height of the CM of each subject. Let  $M_{subject}$ ,  $V_{subject}$ ,  $H_{subject}$  be the subject mass, CM velocity, and CM height respectively. Then the constant  $N_{subject}$  has the same units as the angular momentum.

The CM height was taken to be the standing height of the CM. It was with this 3D location that subsequent average velocities were calculated. Once the angular momentum has been normalized participant independent curves for each task be compared.

## 2. Horizontal ground reaction force predictions

An important hypothesis in this work is that the angular momentum about the CM is regulated to zero for transient tasks, i.e.  $L(t) \approx 0$ , where  $L(t)$  is the angular momentum at time  $t$ . To test the validity of this assumption for transient motions we derived a relationship between horizontal ground reaction force, whole-body CM, and CP with the zero-moment assumption. Then the predicted zero-moment forces were compared to the ground reaction forces measured from the force plates, in a similar fashion as was done for the case of level ground steady-state walking in [6].

Let  $\vec{T}|_{hor} = (T_x, T_y) = (T_{CM} \cdot \vec{i}, T_{CM} \cdot \vec{j})$  be the horizontal momentum projected into the frame of the CM. Then the total angular momentum about the CM may be written as;

$$(12) \quad \vec{T}|_{hor} = [(\vec{r}_{CP} - \vec{r}_{CM}) \times \vec{F}]_{hor} = \frac{d\vec{L}}{dt}|_{hor},$$

where  $\vec{F}$  is the ground reaction force, and  $\vec{r}_{CP}$  is the location of the  $CP$  on the ground. For the  $CP$  measured relative to a reference point on the force plate in lab coordinates, the position is written as;

$$(13) \quad x_{CP} = -\frac{M_y}{F_z},$$

and

$$(14) \quad y_{CP} = -\frac{M_x}{F_z},$$

where  $F_z$  is the component the ground reaction force in the  $Z$  direction,  $M_x, M_y$  are the moments about the same point in the lab coordinates.

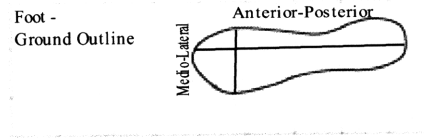


Figure 2: An outline of a foot on the ground. The medio-lateral direction corresponds to the  $X$  direction and the anterior-posterior corresponds to the  $Y$  direction.

Then we solved Eqn. 12 for the horizontal ground reaction forces;

$$(15) \quad F_x = \underbrace{\left[ \frac{F_z}{z_{CM}} (x_{CM} - x_{CP}) \right]}_{F_x^{zero-moment}} + \underbrace{\left[ -\frac{T_y}{z_{CM}} \right]}_{F_x^{moment}}$$

$$(16) \quad F_y = \underbrace{\left[ \frac{F_z}{z_{CM}} (y_{CM} - y_{CP}) \right]}_{F_y^{zero-moment}} + \underbrace{\left[ -\frac{T_x}{z_{CM}} \right]}_{F_y^{moment}}$$

where  $T_x$  and  $T_y$  are the moments about the  $CM$  in the medio-lateral ( $X$ ) and anterior-posterior ( $Y$ ) physiologic directions as depicted in Fig. 2. The two terms in equations 1516 are the explicit

contributions of zero-moment and horizontal moment forces to the ground horizontal ground reaction force. Then to evaluate our hypothesis that the observed ground reaction forces can be mostly explained through a zero-moment analysis we compared  $F_x^{zero-moment}$  and  $F_y^{zero-moment}$  to observed ground reaction forces measured from a force-plate. Eqns 1516 were derived assuming that we have calculated the  $CM$  of the body in lab coordinates, the experimentally determined  $CP$  and the  $F_z$  obtained from the force-plate.

**2.1. Comparing estimated and observed horizontal forces.** In order to assess the amount of agreement between the predicted zero-moment model and the experimentally determined horizontal forces, we used coefficient of determination,  $R^2$ . The definition of the value we use here is  $R^2 = 1$  if there is perfect agreement between the estimated horizontal forces on the  $CM$  and the experimentally determined values. A value of  $R^2 = 0$  indicated the estimated value is worse than the mean value taken from the experimental data.

$R^2$  was calculated as<sup>5</sup>;

$$(17) \quad R^2 = 1 - \frac{\text{residual sum of squares}}{\text{the total sum of squares}}$$

$$(18) \quad = 1 - \frac{\sum_{i=1}^{N_{trials}} \sum_{j=1}^{N_{percent}} (\vec{F}_{exp}^{ij} - \vec{F}_{mod}^{ij})^2}{\sum_{i=1}^{N_{trials}} \sum_{j=1}^{N_{percent}} (\vec{F}_{exp}^{ij} - \bar{F}_{exp}^{ij})^2},$$

where  $\vec{F}_{exp}^{ij}$  and  $\vec{F}_{mod}^{ij}$  are the forces taken at the  $j$ th% of completion of the task of the  $i$ th trial for the experimental and data produced from the model prediction. The value  $\bar{F}_{exp}$  is the grand mean over all trials for the particular task and task percentages, or;

$$(19) \quad \bar{F}_{exp} = \frac{1}{N_{trial} N_{percent}} \sum_{i=1}^{N_{trial}} \sum_{j=1}^{N_{percent}} \vec{F}_{exp}^{ij}$$

**2.2. Center of pressure predictions.** Another way to estimate the amount for quantifying the degree to which angular momentum is regulated about the  $CM$  is to estimate the  $CP$  position and compare this with the location of the  $CMP$  introduced in Chapter 2 in Def. 3 during each transient task.

<sup>5</sup>This  $R^2$  accepts some negative values. In order to prevent this problem the final  $R^2$  value was calculated using the matlab© command.

From Def. 3 it can be seen that when the location of the *CMP* and the *CP* diverse there is a non-zero moment about the *CM* and a zero moment when the two points coincide, Fig. 1. Note that the *CMP* can leave the ground support base while the *CP* cannot. Further, since we calculated the *CMP* using the equations following Def. 3, it clear that the *CMP* can only leave the ground support base when there are non-zero moments acting about the *CM*.

We first plotted the both ground reference trajectories in the ground plane to qualitatively assess the moments acting about the *CM*. Then we computed the mean separation between the *CMP* location and the *CP* normalized by the foot length across the length of the task. Note that if the angular momentum about the *CM* is small then the *CMP* should coincide with the *C* taken directly from the force-plates.

### 3. Segmental contributions to the whole-body angular momentum

In this section we described the method by which we test the hypothesis that whole-body angular momentum remains small throughout each transient. This was observed to be the case in [6] for the case of level ground walking. We extend their analysis for the case of transient motions. Principal component analysis is applied directly to the covariance matrix of the time-series data for angular momentum of each segment to assess the amount of cancellation in each physiological plane. The following is the order of the analysis we undertook;

- (1) Obtained PCs for the segmental angular momenta and the amount of variance explained by each PC.
- (2) Calculated the weighting coefficients (or tuning coefficients) for each PC.
- (3) Determine the amount of cancellation in each spatial direction and therefore the strategy employed by the body to regulate the *CM*.

**3.1. Principal component analysis of the human body model.** PCA or Principal Component Analysis is a common dimension reduction method that has been recently applied to a human body model for level-ground walking [6][10]. Here we describe how we used this method in a similar fashion for transient motions. This was used for two purposes. The first is to find those segments that have the most importance in producing angular momentum about the *CM*. The second is to quantify the amount of segmental cancellation is occurring despite relatively large segment angular momentum.

Since very few components are needed to explain most of the variance this shows that the angular momentum produced by certain limbs is an important variable in bipedal motion. The observations obtained from each link's angular momentum, associated with the kinematic data of a trial, was used to perform a PCA dimension reduction. Using this method, the dimensionality of the angular momentum space, in each cardinal direction is the number of segments in the human body model, i.e.  $N = 16$  for each direction. The total size of the configuration space for angular momentum is  $3N = 48$ .

The components of spin angular momentum are listed in the following order:  $c_1 =$  Left Foot,  $c_2 =$  Right Foot,  $c_3 =$  Left Shin,  $c_4 =$  Right Shin,  $c_5 =$  Left Thigh,  $c_6 =$  Left Hand,  $c_7 =$  Right Hand,  $c_8 =$  Right Thigh,  $c_9 =$  LeftForearm,  $c_{10} =$  RightForearm,  $c_{11} =$  LeftUpperarm,  $c_{12} =$  RightUpperarm,  $c_{13} =$  UpperTorso,  $c_{14} =$  LowerTorso,  $c_{15} =$  Neck,  $c_{16} =$  Head.

PCA was performed on each link's angular momentum for each cartesian direction. The eigenvalue problem, the SVD, was computed using a  $16 \times 16$  covariance matrix. Then the eigenvalues were ordered by their magnitude. Then from the eigenvectors a new 16 dimensional orthonormal basis was obtained with vectors,  $\vec{P}_i$  that are linearly independent and ordered by the magnitude of their associated eigenvalue.

Given the time-series data for the components  $c_i(j)$  for  $i = 1 \dots 16$  and  $0 \leq j \leq T$ , where  $T$  is the total length of the trial, we subtracted out the mean,  $m_i = \sum_{j=1}^t c_i(j)$  to center the data set

$$\hat{c}_i = c_i - m_i,$$

for each  $i$ .

Then we formed the multivariate data matrix,

$$\mathbf{D} = \begin{pmatrix} \hat{c}(1)_1 & \hat{c}(1)_2 & \dots & \hat{c}(1)_{16} \\ \hat{c}(2)_1 & \hat{c}(2)_2 & \dots & \hat{c}(2)_{16} \\ \vdots & & & \vdots \\ \hat{c}(T)_1 & \hat{c}(T)_2 & \dots & \hat{c}(T)_{16} \end{pmatrix},$$

that is assumed to be full-rank (each segment represented in the columns of the data matrix are linearly independent ).



From this matrix we form the covariance matrix where the main diagonals contained the variances of each segment, and the off diagonal contained the covariances between different segments.

$$\mathbf{R}_C = \begin{pmatrix} E[\hat{c}_1\hat{c}_1^h] & E[\hat{c}_1\hat{c}_2^h] & \dots & E[\hat{c}_1\hat{c}_{16}^h] \\ E[\hat{c}_2\hat{c}_1^h] & E[\hat{c}_2\hat{c}_2^h] & \dots & E[\hat{c}_2\hat{c}_{16}^h] \\ \vdots & & & \vdots \\ E[\hat{c}_{16}\hat{c}_1^h] & E[\hat{c}_{16}\hat{c}_2^h] & \dots & E[\hat{c}_{16}\hat{c}_{16}^h] \end{pmatrix},$$

where  $E$  is the expectation,  $h$  denotes the Hermitian, and  $\hat{c}_i = \begin{pmatrix} \hat{c}(1)_i \\ \hat{c}(2)_i \\ \vdots \\ \hat{c}(T)_i \end{pmatrix}$ .

Then we can factor the matrix,  $\mathbf{R}_C$  such that  $\mathbf{R}_C = \mathbf{U}\mathbf{\Lambda}\mathbf{U}^T$ , where  $T$  is the matrix transpose and where  $\mathbf{U}$  and  $\mathbf{\Lambda}$  are the eigenvector and the eigenvalue matrices, respectively.

The eigenvectors of  $\mathbf{R}_C$  are ordered on the basis of how large their corresponding eigenvalues are. The maximum variance is the largest eigenvalue and the minimum variance is the smallest eigenvalue of the angular momentum time-series data. The first two eigenvectors,  $\vec{PC}_1$  and  $\vec{PC}_2$  define the best-fit plane of angular momentum variance. The third eigenvector  $\vec{PC}_3$  defines the plane's normal direction which results in a space of segmental angular momentum.<sup>6</sup>

Each segment can be placed in this space as a linear combination of each of the principal components. The amount of variance we wish to explain is used as way to indicate the number of principal components that were needed to explain a particular piece of data. This gave us a way to understand how much of an effect a particular segment is having on the underlying data.

As an example, consider the segmental angular momentum from the leg and the head. The right foot is much more involved in normal walking, in terms of angular momentum, than the head. Therefore, if we view the three PCs that explain greater than 90% of the data in  $\mathbb{R}^3$  then the distance from the origin to the point representing the right foot would be much greater than that of the head in this segmental angular momentum space we have now defined.

---

<sup>6</sup>For the walking the number of components needed for 2 of the three directions was three. This gives a nice way to visualize segments in this latent space. For some movements 4 PC's might be needed to obtain requisite data explained.

Another important note on the interpretation of the PCA results is it shows how particular segments actually cancel the variance in particular directions. This is most evident in the case of walking where the left and right foot will have similar, opposite signed, variance explained by the first PC. This comes from the fact that the movement of the right leg is tightly coupled, statistically, with the left leg. This is because one leg's angular momentum cancels the angular momentum of the opposite leg through the gait cycle in order to keep moments about the  $CM$  small.

**3.2. Calculation of Tuning Coefficients.** The relevant PCs have been obtained. They can be represented in the following manner as a sum;

$$(20) \quad \vec{\Lambda}_j(t) = \sum_{i=1}^N C_j^i(t) \cdot \vec{P}_j^i,$$

where  $N = 16$  is the number of segments in the model and  $C_j^i(t)$  with  $t \in (0, 100)$  are time-dependent tuning coefficients. However, to obtain the dependence of each segment on a particular physiological direction we introduced a normalized tuning coefficient  $c_j^i(t)$  [6], such that:

$$(21) \quad \vec{\Lambda}_j(t) = \left( \sqrt{\sum_{i=1}^N (C_j^i(t))^2} \right) \sum_{i=1}^N c_j^i(t) \cdot \vec{P}_j^i,$$

where the term in parentheses is the magnitude of the angular momentum vector in  $N$  dimensional segment space. In addition the tuning coefficients are normalized so that  $\sum_{i=1}^N |c_j^i(t)|^2 = 1$ ,  $\forall j = 1 \dots 3$ ,  $t \in (0, 100)$ .

Then PCA was performed to find the smallest number of principal components that explained greater than 90% of the variance in angular momentum reported from the model. This was done in two different ways to capture the amount of inter and intra-subject variability in the model. For participant dependent measures, analysis was performed on each subject with 10 trials each. For participant independent measures, analysis was performed on all subjects comprising a total of 50 trials for each task.

**3.3. Calculation of segmental angular momentum cancellation.** The amount of cancellation for each participant can be calculated in each physiological direction,  $i = 1 \dots 3$  by;

$$(22) \quad S_j = 1 - \sqrt{\sum_{i=1}^{N_E} DE_j^i \left[ \frac{\sum_{q=1}^N P_j^{iq}}{\sum_{q=1}^N |P_j^{iq}|} \right]^2}$$

where  $q = 1 \dots N$  and where  $N_E = 5, 9, 4$  (for walking, turning, and starting, respectively) is the level precision considered in this study. The data explained,  $DE_j^i$  were considered weights in 22 the net cancellation of each orthogonal direction is a sum of squares.



## Results

### 1. Normal Walking in Sagittal Plane

In order to establish a baseline from which we can compare other motions, we analyzed whole-body angular momentum during straight level ground walking. Each subject was asked to walk at  $1.5 \frac{m}{s}$  through the capture volume. These data were then processed to include whole-body angular momentum for 0% to 100% gait cycle.

The maximum deviation observed in the whole body angular momentum, Fig.1 was at maximum  $\approx 0.01$  normalized units. This agrees with the observations made by [6] that the whole-body angular momentum about the *CM* is a tightly regulated quantity during walking. This indicated whole-body angular momentum over the whole gait cycle was tightly regulated in the sagittal direction. Each other direction; coronal and transverse directions saw very tight regulation during walking as well.

Note that in Table 1 the first principal component explained,  $DE_x^1 = 89.8\%$  of the variance observed in sagittal direction during angular momentum straight walking data. In the medio-lateral direction, the first PC explained  $DE_y^1 = 63.7\%$  of the data.

Note that in Fig. 2 the sagittal direction (first bar plot) contributions for both limbs, over the whole gait cycle, were roughly equal and opposite. This result followed from the cyclic nature of walking with each leg producing an ideally equal amount of angular momentum about the CM over one gait period.

During level ground walking the ground reference trajectories the angular momentum about the CM is tightly regulated. This can be seen in Fig. 3 where the CMP (green) tracks the horizontal moments being applied to the CM (blue). The placement of each foot, indicated by the red CP, follows the expected path determined to be part of a normal gait cycle.

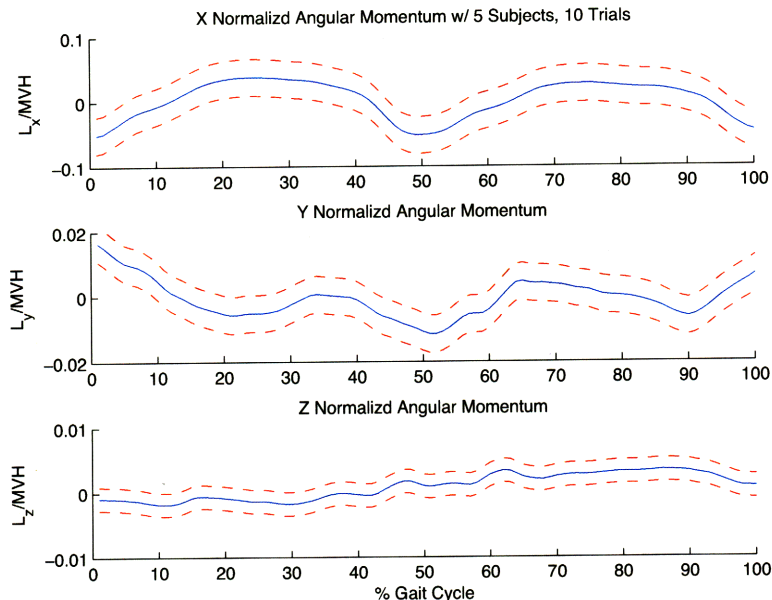


Figure 1: The whole-body angular momentum. Values are normalized by  $M \cdot V \cdot H_{subject}$ . This is an average of 5 participants with 10 trials walking at a fast pace 1.5 m/s in the saggittal direction. Red dashed lines indicated a standard deviation above and below the mean of the angular momentum data in blue.

Table 1: Data Explained in walking for 10 Trials Per Subject over one gait cycle

Participant	$DE_x^1$	$DE_y^1$	$DE_z^1$	$DE_x^{III}$	$DE_y^{III}$	$DE_z^{III}$	$S_x$	$S_y$	$S_z$
JaMa	89.9	57	91	99	87	97.5	0.92	0.80	0.84
AlGr	89.5	55.6	94.7	99.1	90.2	98.2	0.74	0.75	0.80
AnMa	87	31	82	99	76.5	94.4	0.71	0.79	0.76
ErMa	90.1	55.8	95.7	99	84.8	98	0.72	0.72	0.88
GrEl	89.8	63.7	89.3	99	93	97.6	0.73	0.68	0.74
<i>mean ± s.d</i>	$89.3 \pm 1$	$52.6 \pm 13$	$90.5 \pm 5$	$99 \pm 0.04$	$86 \pm 6$	$97.1 \pm 1$	0.72	0.79	0.76

## 2. Left Inside Turn Results

Turns can come in several varieties; there are turns on the inside foot and turns on the outside foot. This thesis focuses on turns taking place in the former style, the inside turn or spin turn [13]. Many times turns will take several steps to complete. However, the spin turn is representative of a type of turn that is quick to perform and is completed in one step. The hypothesis is that

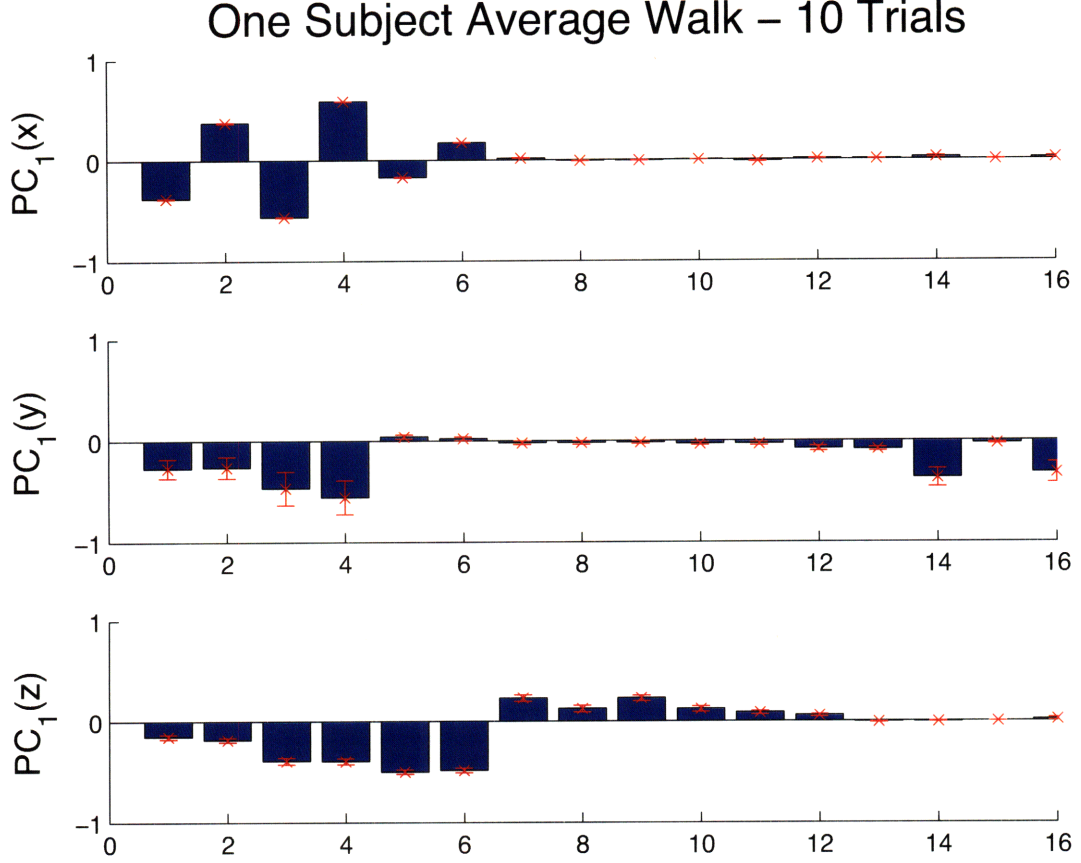


Figure 2: The three direction for the first PC for straight walking at 1.5 m/s. The components are in order from 1 - 16 : left foot, right foot, left shin, right shin, left thigh, left hand, right hand, right thigh, left forearm, right forearm, left upper arm, right upper arm, lower torso, upper torso, neck, and head. Note that the contributions from each lower limb over the whole gait cycle is roughly equal. Walking is cyclic and over one gait cycle. Note that each limb makes an roughly equal contribution to total whole-body angular momentum.

contributions to the whole-body angular momentum about the center of mass are tightly regulated during one *Turn-Cycle* and that segmental contributions are not symmetrically cancelled.

DEFINITION 4 (Turn/Inside Turn/Spin Turn). *The heel-strike on the step preceding the pivot foot heel-strike to the toe-off at the end of step completion. Similar to the notion of a gait cycle in level ground walking, there is a turn cycle that is composed of a heel-strike with a particular heel*

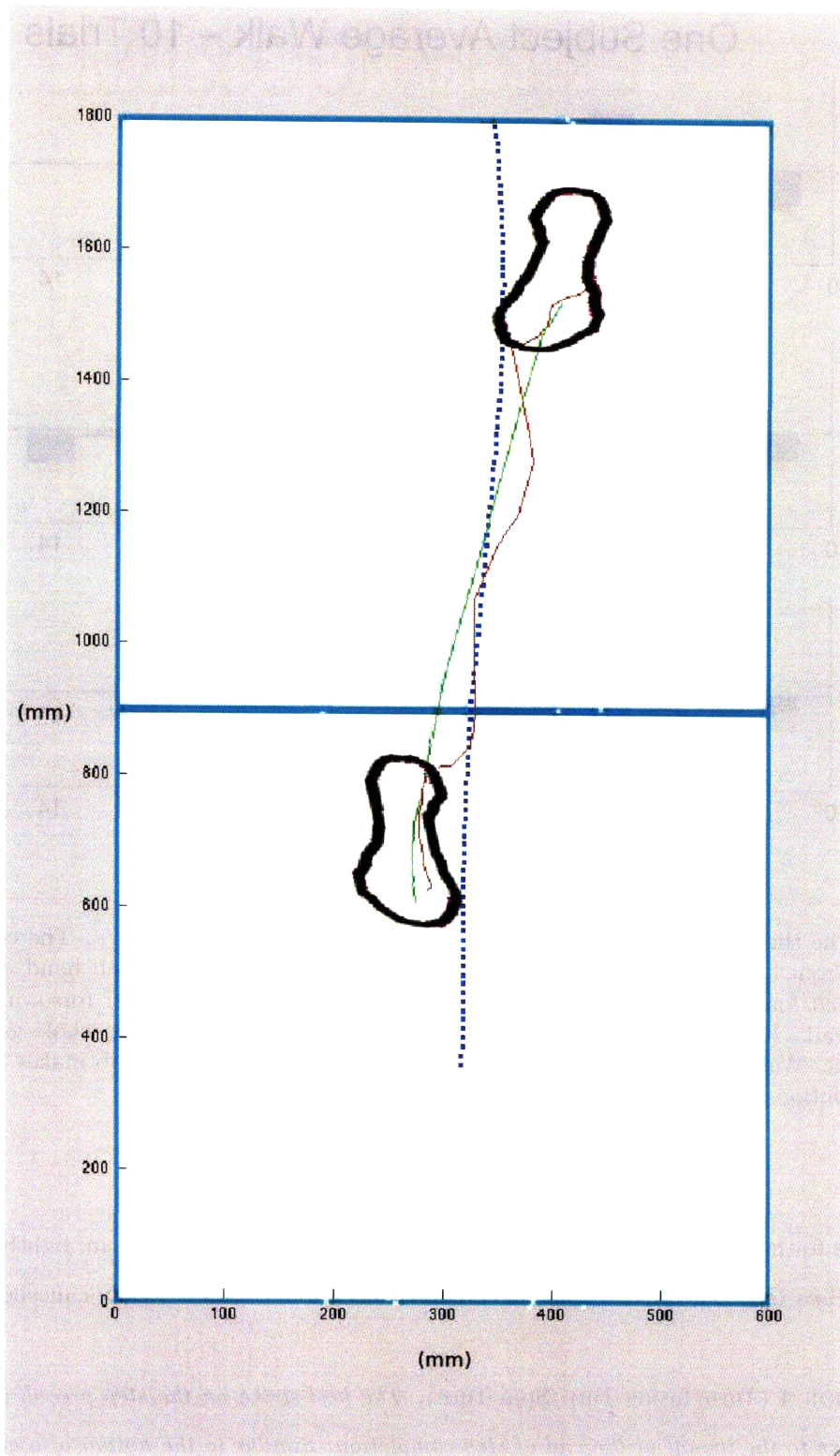


Figure 3: Ground reference trajectories CP (green), CMP (red) and CM (blue) during walking straight. Note that the CP and CMP stays within the foot during stance on each foot. This is in agreement with previous observations of ground reference trajectories during level ground walking.



Participant Independent Analysis – Walk Fast – 50 Trials

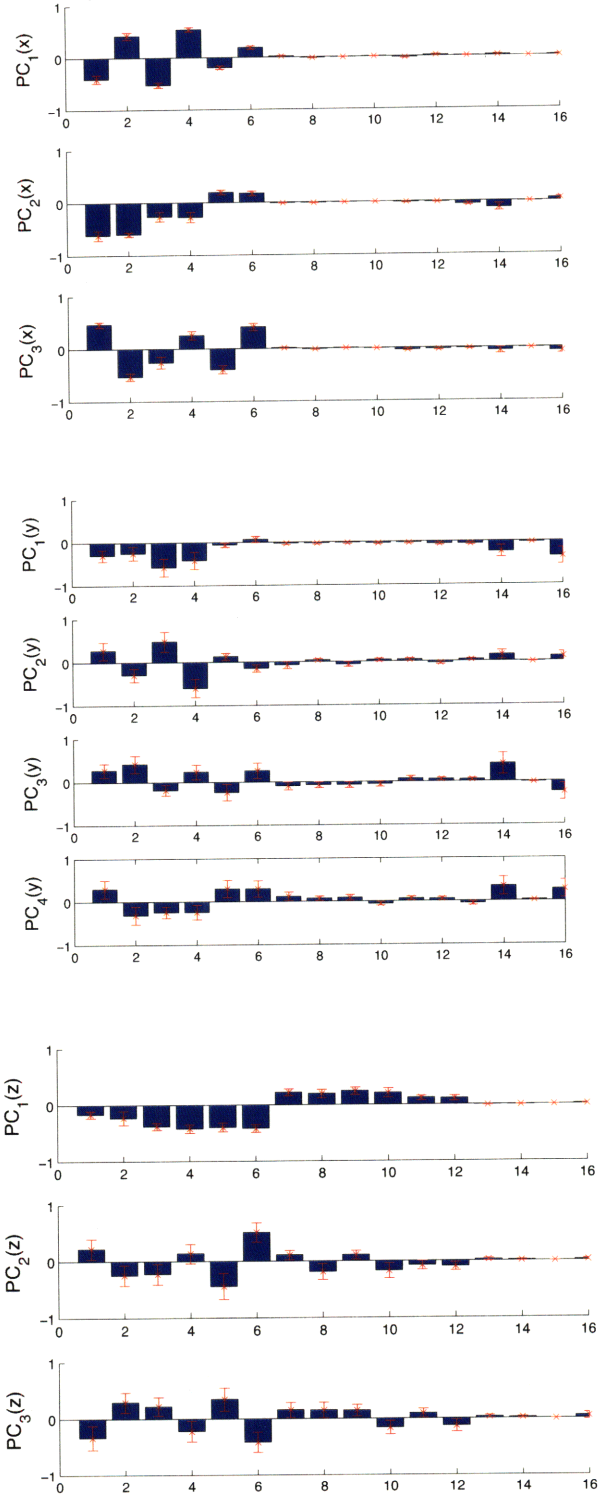


Figure 4: Participant-Independent Results for the first three PCs of each trial that account for more than 90% of the variance observed in data for walking straight at 1.5 m/s. The data explained by each PC for: (X): 85.3%, 10.3%, 2.1%; (Y): 82.8%, 9.6%, 4.4%; (Z): 88.4%, 6.2%, 4.3%.

and completed when that same heel strikes the ground again after swing, see Chapter 3, Fig. 1 for a depiction of that turn.

**2.1. Whole-Body Angular Momentum in Turning.** In a turn of the type we have defined, the whole-body angular momentum is tightly regulated. Also, the amount of segmental cancellation of the lower limbs is less than that observed in walking, either with these participants or with those reported in [6]. This suggested a strategy that involves the body regulating its whole-body angular momentum and using the muscles to produce moments about the  $CM$  with the swing foot during the foot-pivoting period of the left-handed turn.

As an illustration for the above definition for turning, with the human body model described in Chapter 3, a participant was asked to turn at  $90^\circ$  and then modeled in Matlab. This trial is depicted in Fig. 8. The ground reference trajectories for a  $90^\circ$  turn are shown in Fig. 9. Qualitatively, it appears that on the first step the  $CMP$  tracks the  $CP$  poorly, indicating there is a moment being applied to the  $CM$  during the first step of the turn. During second step, the pivot foot, the  $CMP$  tracks the  $CP$  reasonably well compared with the initiating step. The latter foot that the turn occurs with, and the preceding step spinning about that foot and driven by momentum produced by the rotating right foot, recovers after the rotation in the transverse plane is completed. This is the strategy that is found via a close examination of the whole-body and segmental contributions to angular momentum about the  $CM$ .

Fig. 5 shows the normalized whole-body angular momentum about the  $CM$  in lab frame coordinates. These values have been scaled by the constant,  $M_{subject}V_{subject}H_{subject}$  as defined in Table 2. These values were computed from kinematic gait data, as defined in Eqn. 11 of Chapter 4. Throughout the entire turn-cycle the the absolute value of the angular momentum mean plus one standard deviation remains smaller than 0.2 in the anterior-posterior direction (X), smaller than 0.05 in the medio-lateral direction (Y) and smaller than 0.02 in the vertical direction (Z), see Fig. 5 for a total of 50 trials (5 subjects  $\times$  10 trials each). This indicated that angular momentum was regulated throughout the turn.

Comparing the result presented in Fig. 5 to those in Fig. 1 of this Chapter, indicated that despite the turn and pivot taking place after double support in the turning trial the whole-body angular momentum remains relatively small. These data indicate that the left inside turn required the body to regulate the  $CM$  position.

**2.2. Segmental Contributions to whole-body angular momentum in Turning.** We conducted two types of analysis on angular momentum data in order to understand segmental contributions to whole-body angular momentum. The first study conducted was a participant-dependent and then participant-independent analysis. The results of the participant-dependent analysis are listed in Table 2.

For all subjects, on average, the first three PCs accounted for  $97.8 \pm 0.1\%$  (X) ,  $96.7 \pm 2\%$  (Y), and  $97.2 \pm 0.7\%$  (Z) directions. A direct comparison of the anterior-posterior (Y) and medio-lateral (X) directions to those observed in walking was not possible because the reference frame was not attached to the subject. However, the vertical (transverse plane) need not travel with the subject through the turn to be comparable with level ground walking.

In both walking and turning, the amount of data explained by the first principal component in the vertical direction, for turning  $DE_{z_{turn}}^1 = 88.4 \pm 3\%$  and for walking  $DE_{z_{walk}}^1 = 87 \pm 2\%$ [6] are very similar. Further, the (Z) component of whole-body momentum for turning and walking is also in nice agreement with similar one standard deviation peaks above the mean at 0.01 normalized units. However, the difference between the two movements is clear upon comparing the vertical component of the first PCs, Fig. 7. In walking, over one gait cycle, the individual lower limb segments contribute similar amounts to the variance of the first PC. However, in turning the right lower limb segments; foot, shin and thigh, contribute the greatest and unequal amount compared to the left lower limb. This suggests a strategy of angular momentum regulation that involves using the right leg for swing during a left inside turn.

**Ground reaction force predictions in a left handed turn.** The ground reaction forces for a left handed turn were obtained with  $R^2$  values as reported in Table 3. Note that the anterior-posterior direction for the turn was in good agreement with the zero-moment hypothesis ( $R_y^2 = 0.94$ ). However, the medio-lateral direction has very poor agreement with the observed force profiles. This can be seen in Fig. 10, where the medio-lateral forces increased when the turn started and the pivot foot pushed off the forceplate in the direction that was previously medio-lateral.

**Normalized Tuning Coefficients in a Left Turn.** The normalized tuning coefficients for a left turn were obtained using Eqn. 13 of Chapter 4. Note that the first PC, for  $< 50\%$ , is positive until the period of double support near the middle of the turn cycle. Compare this with the tuning

coefficient in the transverse plane, where for the first  $< 50\%$  the first PC is negative until the end of the trial where it increases to a maximum around  $60\%$ . This is in agreement with the task itself; the turn combines characteristics of level ground straight walking and a turn to the left right after double support.

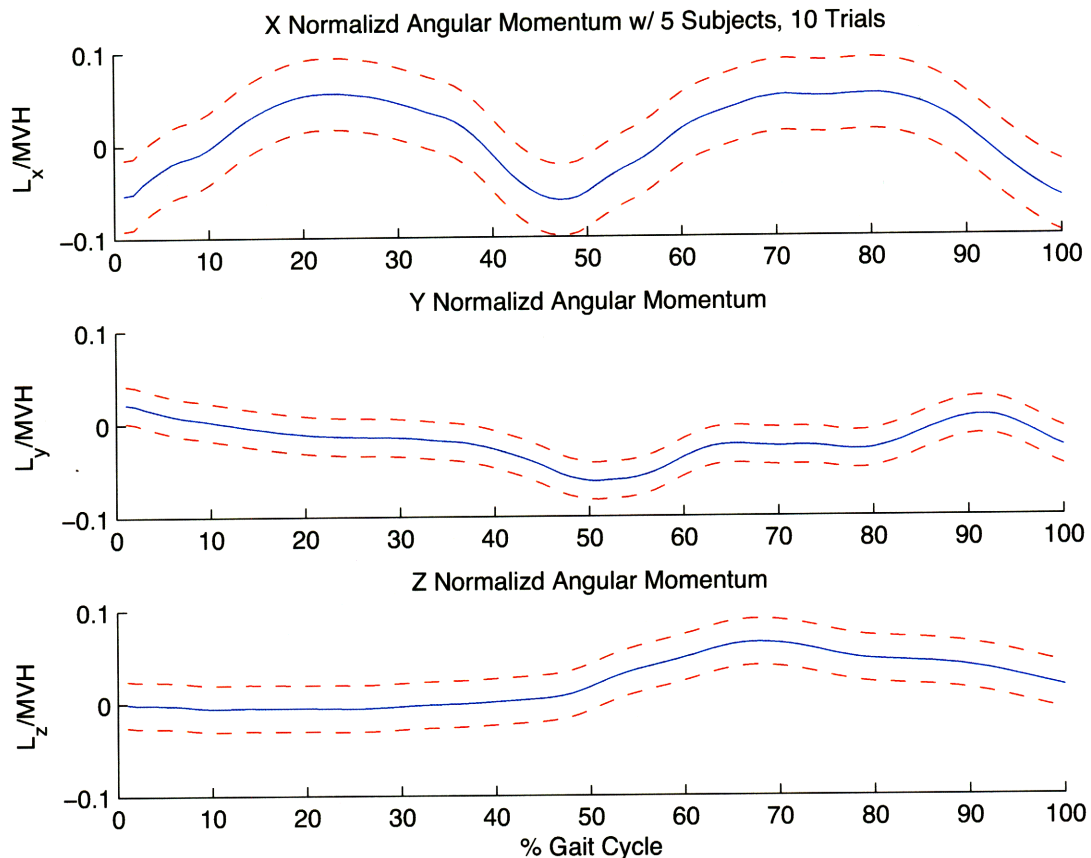


Figure 5: Whole-body angular momentum averaged across 5 participants with 10 trials/participant for a Turn. This results in a total 50 trials. Each curve was normalized by the mass, velocity, and height of the  $CM$  through the turn, see Table 2 for values. The red-dotted lines are one standard deviation above and below the mean.

### 3. Rapid Starts from Neutral Pose

Abrupt starts, or rapid accelerations from standing, exist throughout most of our day. It requires the complex interaction of muscle synergies throughout the lower body. In particular the

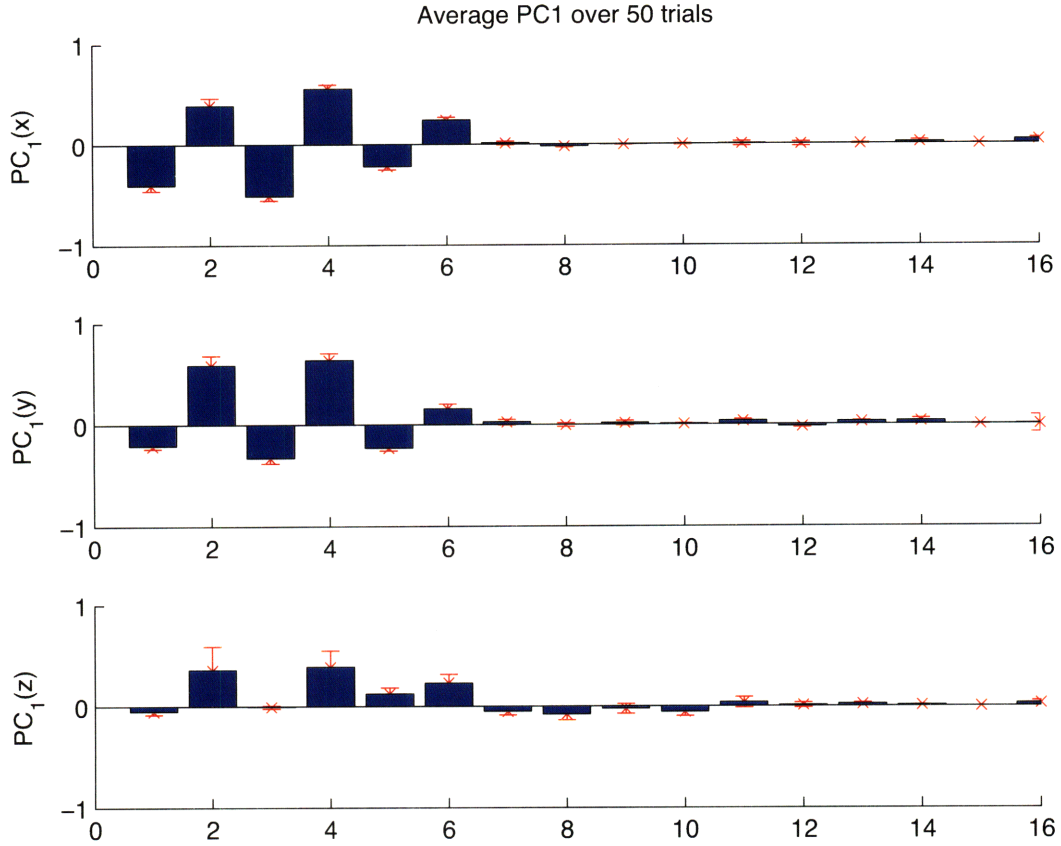


Figure 6: The three directions for the first PC for turning averaged for 5 participants taking 10 turns each. The components are left foot(1), right foot(2), left shin(3), right shin(4), left thigh(5), right thigh(6), left hand(7), right hand(8), left forearm(9), right forearm(10), left upper arm(11), right upper arm(12), lower torso(13), upper torso(14), neck(15), and head(16). Note that PC1 of the Z direction has segments that contribute a large unbalanced amount of angular momentum about the  $CM$ . The components that do this correspond to the right foot, shin and thigh.

recruitment of the thighs, and lower legs to produce moments of force about the ankles and hips. These forces cause the  $CM$  and  $CP$  to diverge propelling the body forward towards the stance limb.

DEFINITION 5 (Rapid Start). *From quiet stance the body accelerates maximally forward causing the  $CM$  to move forward and push the body towards the left lower limb to recover and continue walking towards a specified target.*

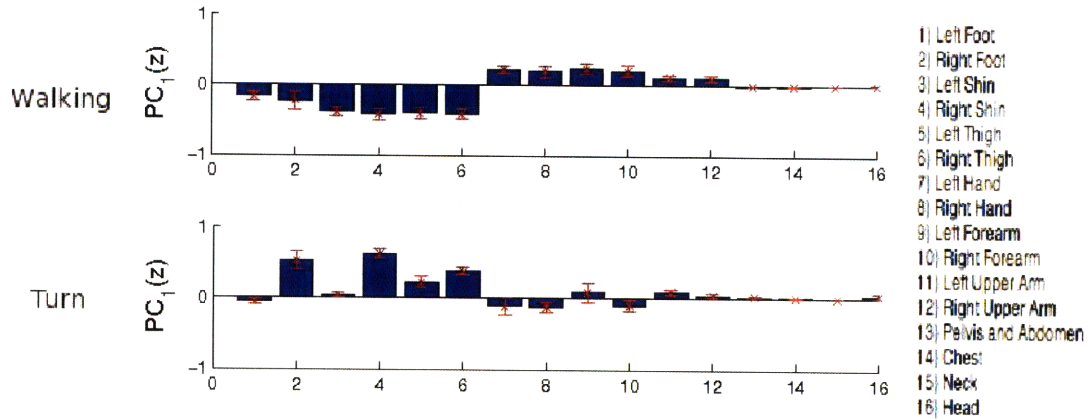


Figure 7: A participant-independent comparison between the variance contributed to the first PC in both Walking (Top) and a Turn (Bottom) in the transverse plane. The right foot contributed a great amount of variance to the first PC than left foot.

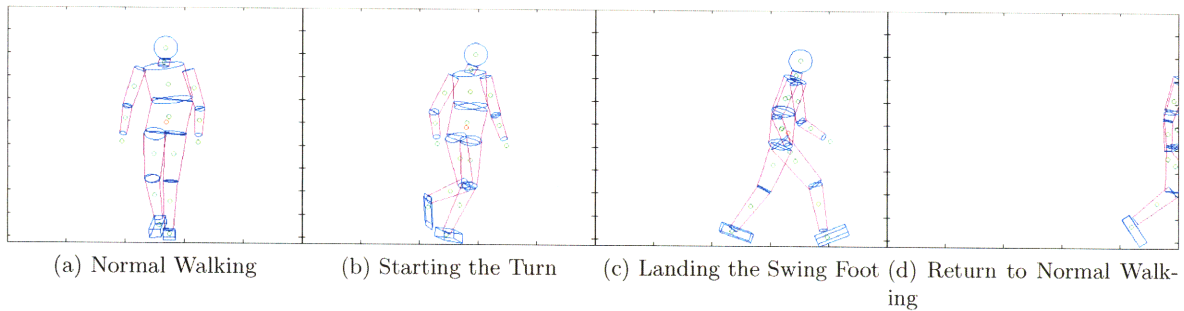


Figure 8: Example Left Turn Trial

The stance limb for this study was the left limb. We assumed symmetry between the left and right leg and that the two legs in our subjects were not substantially different.<sup>1</sup> This study was done to find an angular momentum strategy for rapid starts, as well test the applicability of the zero-moment strategy during a rapid start. An example of the anthropomorphic reconstruction of the body from marker data can be seen in Fig. 13.

Fig. 14 shows the whole-body angular momentum curves associated with a rapid start. The  $CM$  appears to be a tightly conserved quantity. The whole-body angular momentum was normalized by the  $MVH$  values in Table 5. The one standard deviation curves above and below the mean do

<sup>1</sup>Changing the start leg could possibly change the outcome of this study if participants were much more practiced in using one leg over the other.

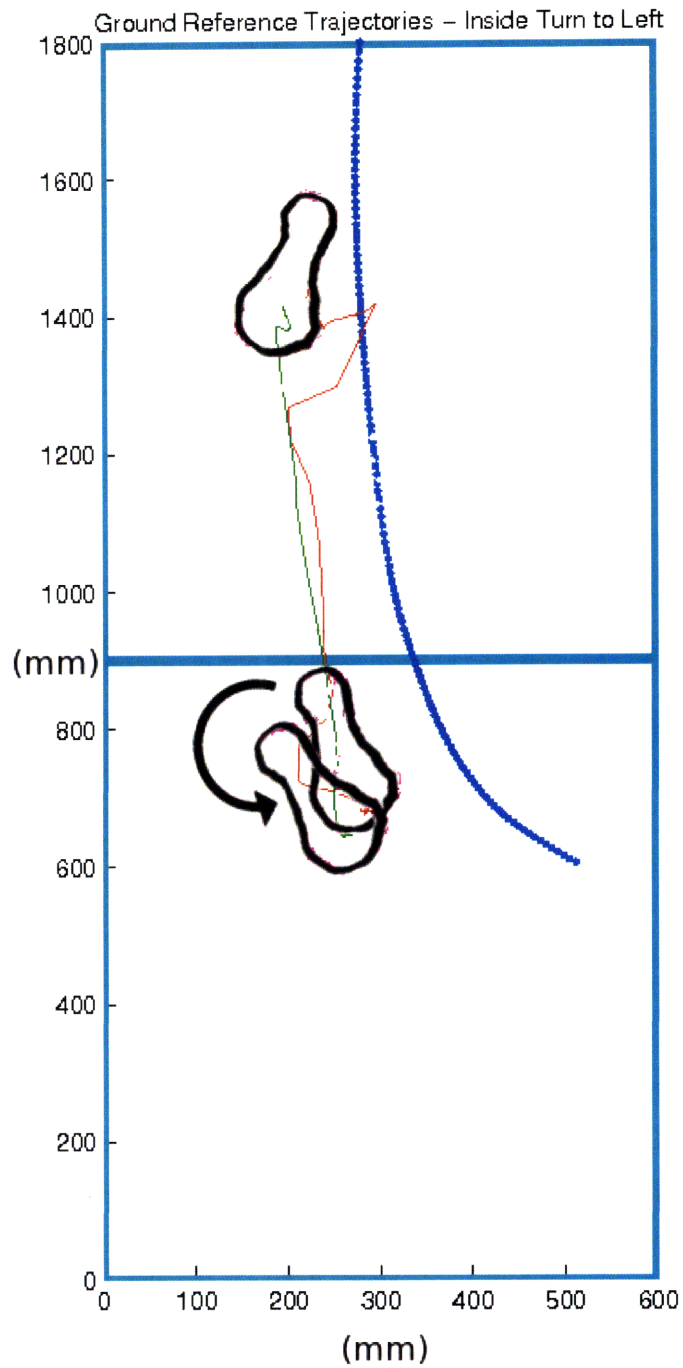


Figure 9: Ground reference trajectories CP (green), CMP (red) and CM (blue) during a turn. Note that the CP and CMP stays within the foot (the markers indicating the fifth metatarsal, the big toe and heel are in pink) during stance on each foot.

Table 2: Data Explained for Turning for 10 Trials Per Subject for one whole Gait Cycle

Participant	$DE_x^I$	$DE_y^I$	$DE_z^I$	$DE_x^{III}$	$DE_y^{III}$	$DE_z^{III}$
JaMa	88.7	87	91.8	98	97.6	97.9
AlGr	85.1	83.1	84.8	97.9	96.7	98
AnMa	83	81.6	88.4	97.8	93.5	96.6
ErMa	83	79.7	88.5	97.7	97.8	96.9
GeEl	86.9	82.6	88.5	97.8	98.1	96.6
<i>mean</i> $\pm$ <i>s.d</i>	$85.3 \pm 3$	$82.8 \pm 3$	$88.4 \pm 3$	$97.8 \pm 0.1$	$96.7 \pm 2$	$97.2 \pm 0.7$
	$S_x$	$S_y$	$S_z$			
	0.83	0.94	0.90			
	0.88	0.82	0.89			
	0.88	0.84	0.87			
	0.90	0.94	0.94			
	0.87	0.95	0.96			
	0.87	0.90	0.91			

Table 3: Body mass  $M_{subject}$ ,  $CM$  height  $H_{subject}$  and average speed through the turn,  $V_{subject}$  for each study participant

Participant	$M_{subject}(kg)$	$H_{subject}$	$V_{subject}$	$R_y^2$	$R_x^2$
JaMa	59	0.94	1.33	0.98	0.18
AlGr	57.6	0.79	1.22	0.95	0.31
AnMa	59	0.97	1.27	0.94	0.10
ErMa	82	1.02	1.23	0.88	0.34
GrEl	83	1.03	1.43	0.95	0.26
<i>mean</i> $\pm$ <i>s.d</i>	$64.4 \pm 12$	$0.93 \pm 0.1$	$1.24 \pm 0.04$	$0.94 \pm 0.04$	$0.24 \pm 0.1$

not go above  $\pm 0.2$  in the (X) direction, 0.05 in the (Y) direction, and  $\pm 0.02$  in the (Z) direction. This suggested that the  $CM$  is a tightly regulated quantity for a rapid start.

For the participant dependent analysis I produced Table 4. Four principal components were needed to explain  $> 90\%$  of the variance observed in the data. Fig. 15 shows the first principal components of the rapid start and each explains,  $73 \pm 9\%$ (X),  $61 \pm 11\%$ (Y) and  $69 \pm 9\%$  (Z), respectively.

The lower limbs dominated in the sagittal (X) direction. However, in the coronal (Y) direction, Fig. 15, the amount of variance contributed by the upper torso and head were nearly the same as that of the lower limbs. This suggests that the legs are canceling the angular momentum produced by the torso during the initial lunge at the beginning of the rapid start.



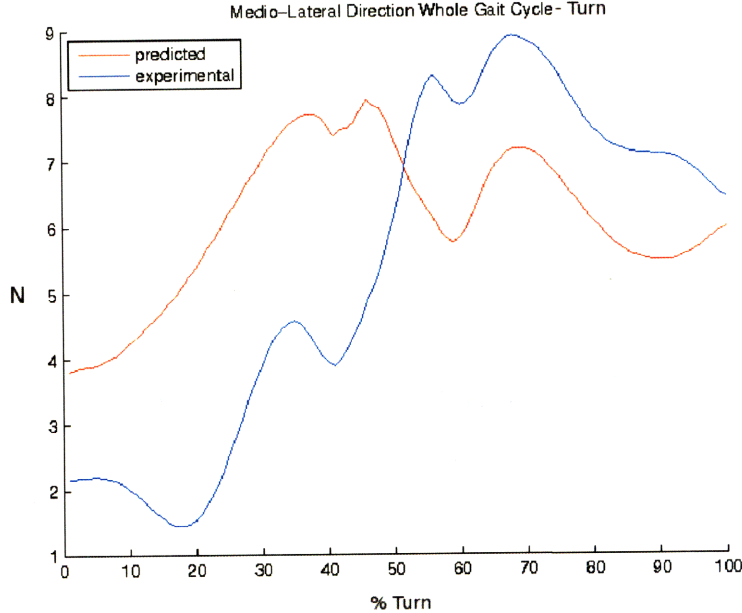


Figure 10: The predicted medio-lateral forces showed poor agreement with experimentally observed values. The increase in the experimental values of the medial ground reactions corresponded to the period when the turn starts after 50% turn-cycle.

The ground reference trajectories in Fig. 16 shows the trajectory these biomechanical points through the rapid start. This reveals some of the adjustments that occurred in the body prior to the rapid start. The rapid start was initiated by a slight rocking of the body to the support limb prior engaging the swing to recover balance after the lunge of the upper torso.

Also, it was interesting that on the second step the *CMP* is outside the approximate region foot support during single stance. This suggests that the moment acting on the *CM* was particularly high at this stage in the start. However, because this is just for one subject it is unclear if this will always be a feature of the rapid start.

**3.1. Horizontal ground reaction force and *CP* predictions in Rapid Starts.** In order to test the applicability for the zero-moment strategy for rapid starts we analyzed ground reaction force predictions from rapid start data. In order to analyze this, data was taken from the double support phase up to the end of single support on the final force plate before heel strike.

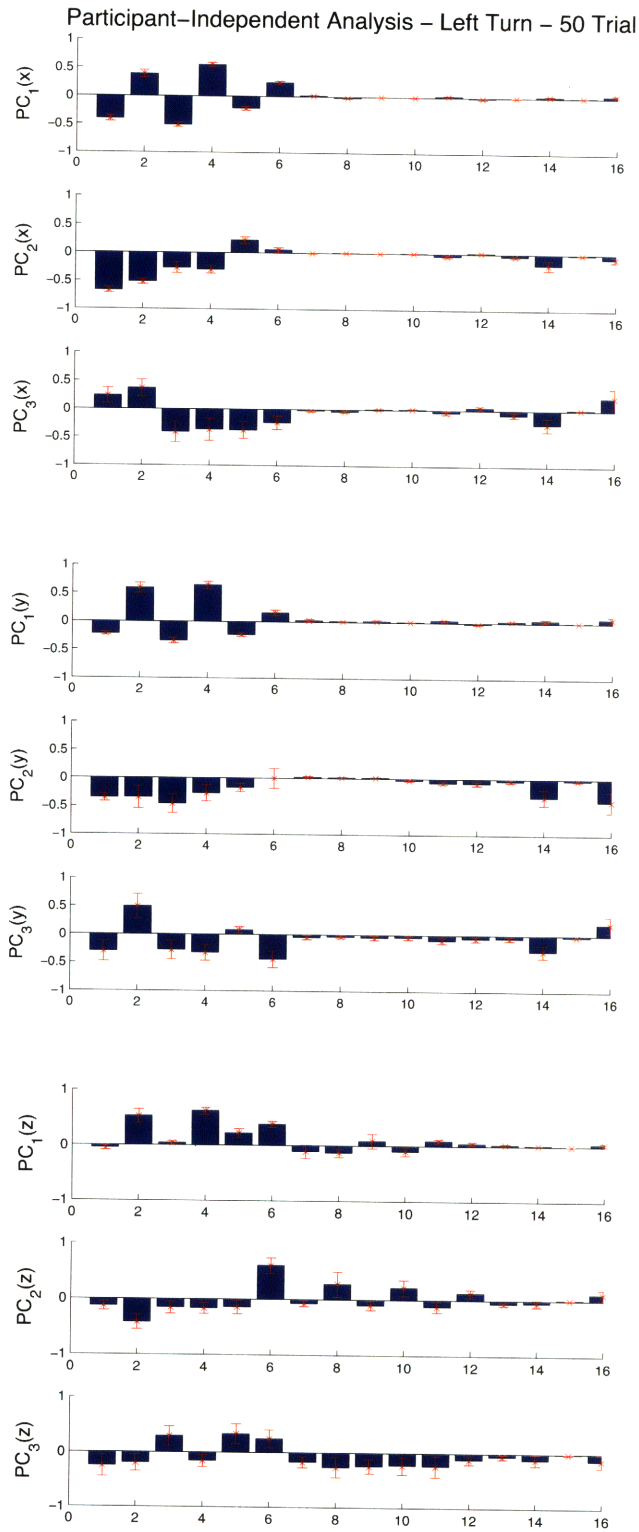


Figure 11: Participant-Independent Results for the first three PCs of each trial that account for more than 90% of the variance observed in the data for turning. The data explained by each PC for: (X): 85.3%, 10.3%, 2.1%; (Y): 82.8%, 9.6%, 4.4%; (Z): 88.4%, 6.2%, 4.3%.

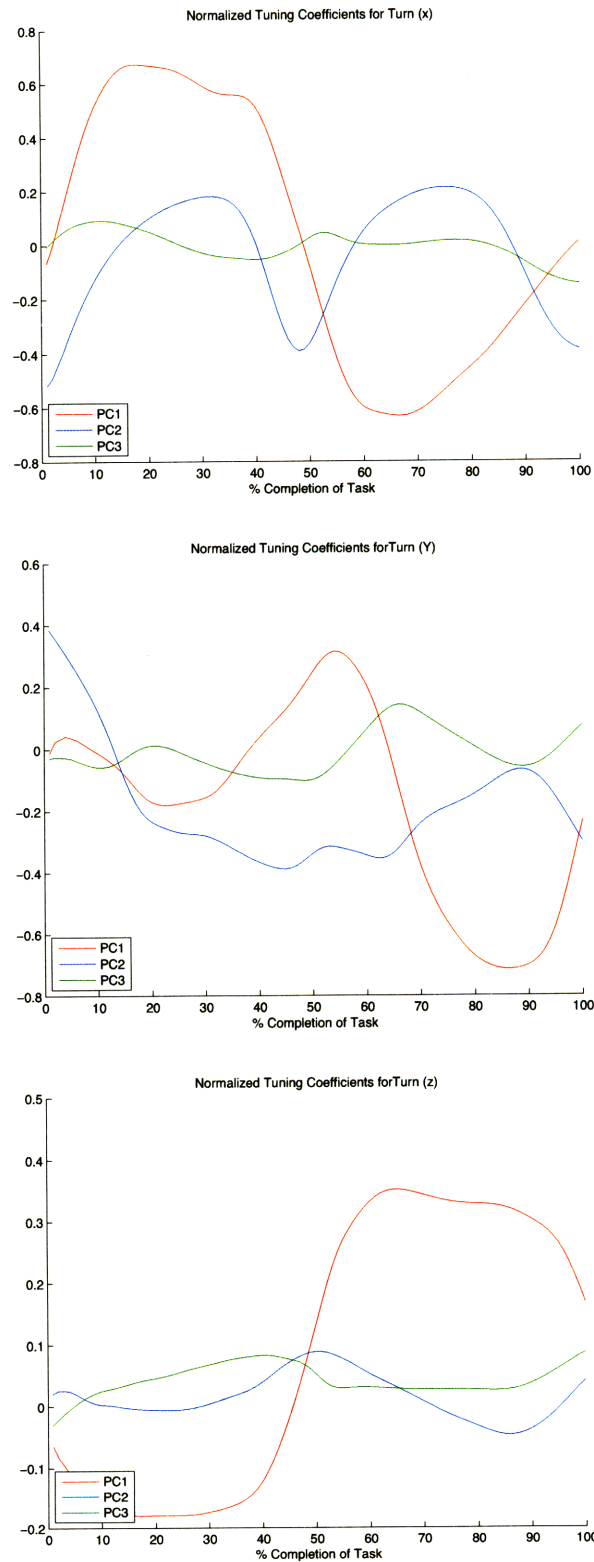


Figure 12: The mean values over all participants and trials of the normalized tuning coefficients associated with a one-step turn to the left. From the top to the bottom are the (X), (Y) and (Z) directions, respectively. These normalized tuning coefficients were obtained using Eqn. 13 of Chapter 4.

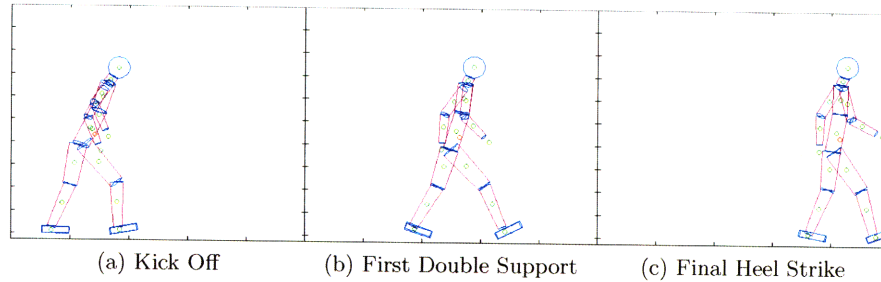


Figure 13: Example Rapid Start

The ground reaction force prediction for double support and single stance showed good agreement for the anterior-posterior direction ( $R_y^2 = 0.86$ ) and similarly good agreement in the medio-lateral direction ( $R_x^2 = 0.86$ ), note Fig. 18. As a comparison, the values reported for the middle 50% of the gait cycle [6] slightly higher ( $R_x^2 \approx 0.91$  and  $R_y^2 \approx 0.90$ ).

**Normalized Tuning Coefficients for Rapid Starts.** Normalized tuning coefficients were derived using Eqn. 13 of Chapter 4 and are depicted in Fig. 19. Similar to the observations made in [6], during walking the first PC become less dominant during the powered plantar flexion phase as the second PC increases dominance.

Table 4: Data Explained in Rapid Starts for 10 Trials Per Subject

Participant	$DE_x^1$	$DE_y^1$	$DE_z^1$	$DE_x^{III}$	$DE_y^{III}$	$DE_z^{III}$
JaMa	80	63.8	79.6	98.9	95.5	97
AlGr	78.5	66.5	78.5	96	92	95.2
AnMa	78	41.2	64	98.1	83	86
ErMa	59.4	67.4	61.6	92.3	88.3	89
GrEl	68.8	65	61	90	90	90
<i>mean ± s.d</i>	$73 \pm 9$	$61 \pm 11$	$69 \pm 9$	$95 \pm 4$	$90 \pm 5$	$91.3 \pm 5$
	$S_x$	$S_y$	$S_z$			
	0.84	0.80	0.85			
	0.82	0.85	0.74			
	0.79	0.69	0.68			
	0.76	0.77	0.86			
	0.92	0.65	0.75			
	<u>0.87</u>	<u>0.75</u>	<u>0.78</u>			

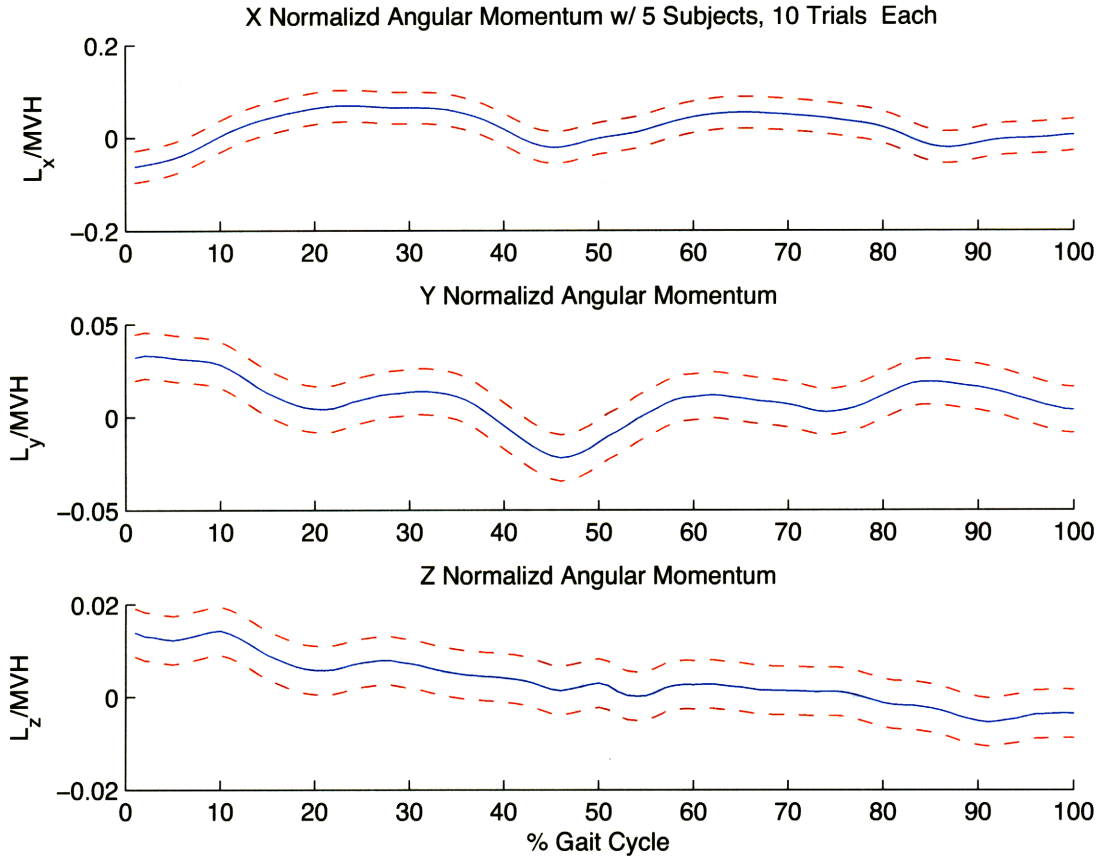


Figure 14: Whole-body angular momentum averaged across 5 subjects with 10 trials each. This results in a total 50 trials. Each curve was normalized by the mass, velocity, and height of the  $CM$  through the turn, see Table 5 for values. The red-dotted lines are one standard deviation above and below the mean.

Table 5: Body mass  $M_{subject}$ ,  $CM$  height  $H_{subject}$  and average speed through the period of rapid starting (including stance prior to start)  $V_{subject}$  for each study participant

Participant	$M_{subject}(kg)$	$H_{subject}$	$V_{subject}$	$R_y^2$	$R_x^2$
JaMa	59	0.82	2	0.73	0.93
AlGr	57.6	0.88	1.6	0.86	0.97
AnMa	59	0.95	1.95	0.92	0.90
ErMa	82	0.92	1.78	0.91	0.67
GrEl	59	0.95	1.95	0.89	0.84
<i>mean ± s.d</i>	$63.3 \pm 10.5$	$0.93 \pm 1$	$1.85 \pm 0.16$	$0.86 \pm 0.07$	$0.86 \pm 0.1$

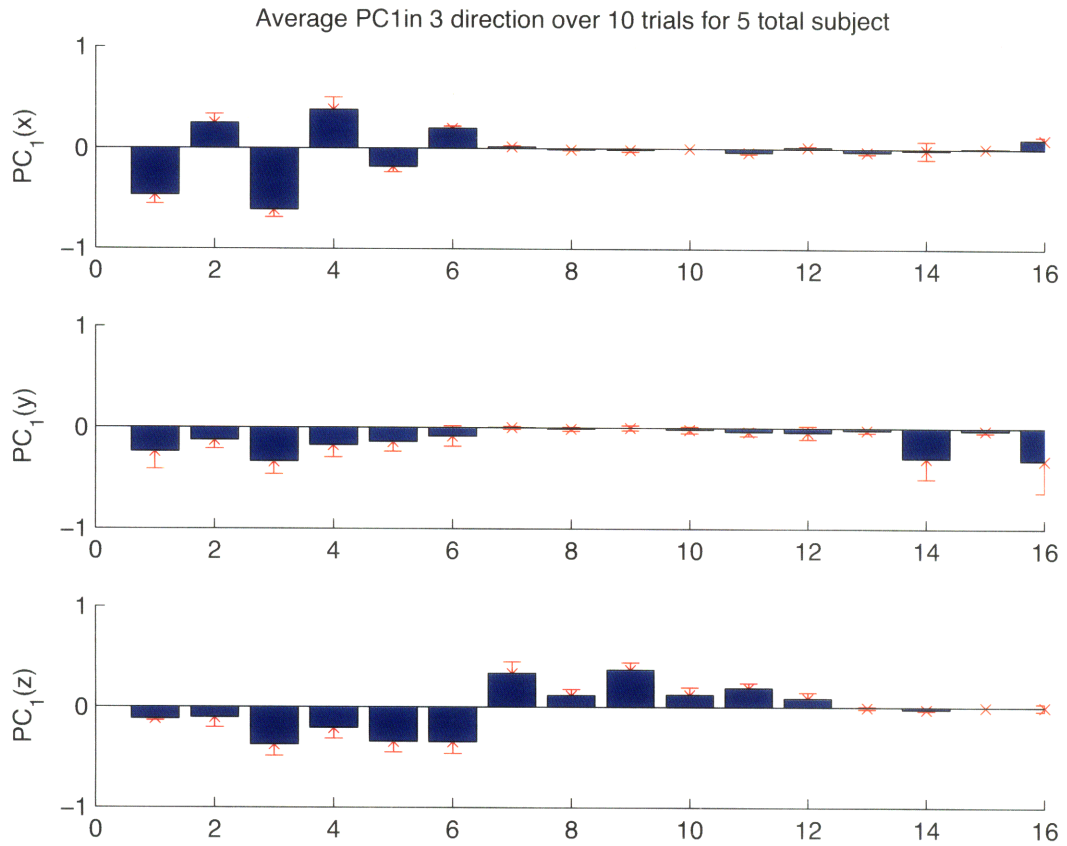


Figure 15: The three direction for the first PC for an abrupt start. Red bars indicate one standard deviation above and below the mean. The components are left foot(1), right foot(2), left shin(3), right shin(4), left thigh(5), right thigh(6), left hand(7), right hand(8), left forearm(9), right forearm(10), left upper arm(11), right upper arm(12), lower torso(13), upper torso(14), neck(15), and head(16).

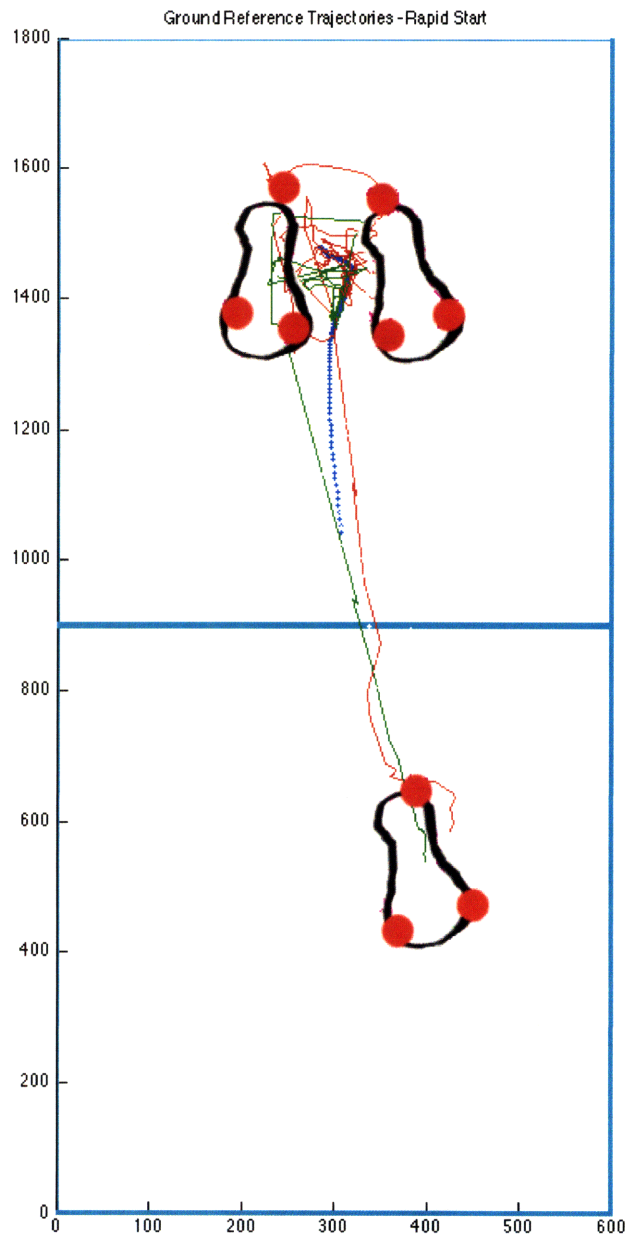


Figure 16: Ground reference points tracking the CM during an abrupt start. The CP, CM, CMP are green, blue, and red respectively. The markers indicate the location of the heel, metatarsil five, and big toe marker.

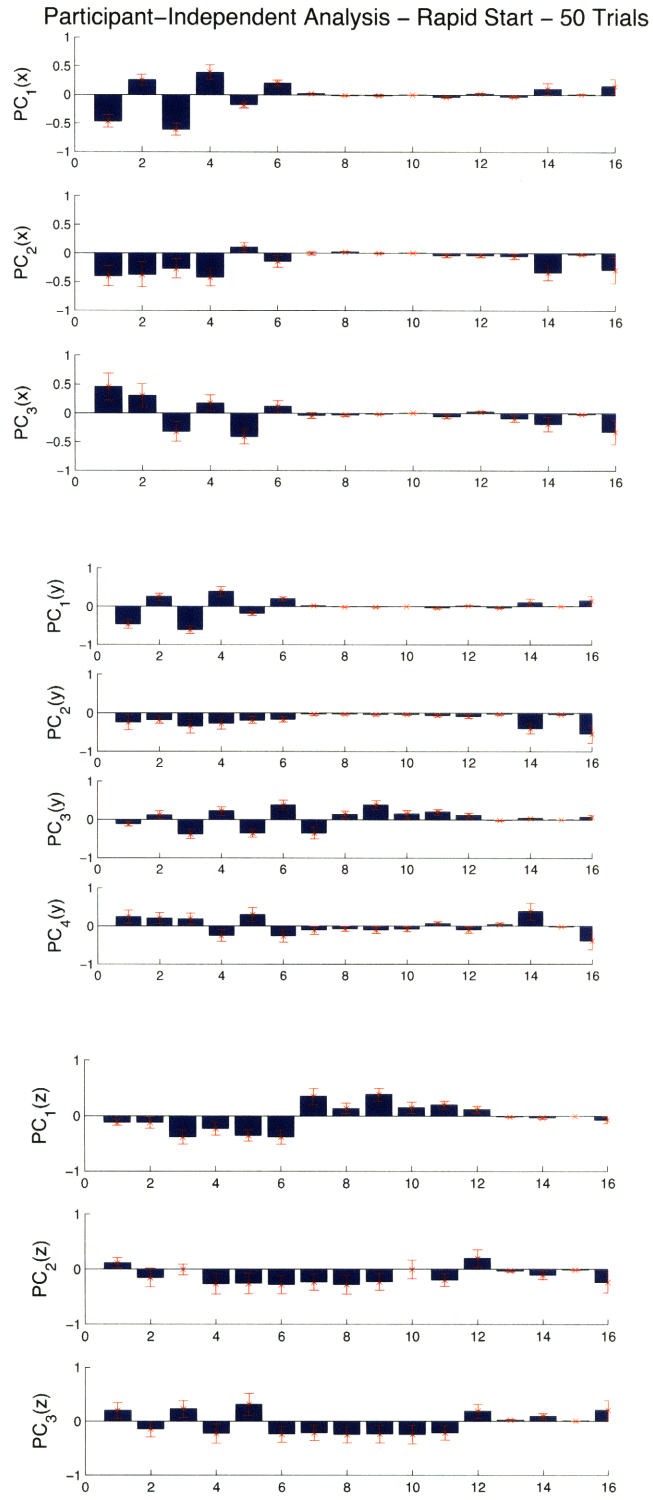


Figure 17: Participant-Independent Results for the first PCs of each trial that account for more than 90% of the variance observed in the data for a rapid start. The data explained by each PC for: (X): 73%, 16.6%, 7.6%; (Y): 52%, 23.1%, 10.4%, 7.1%; (Z): 69.9%, 16.7%, 6.6%.



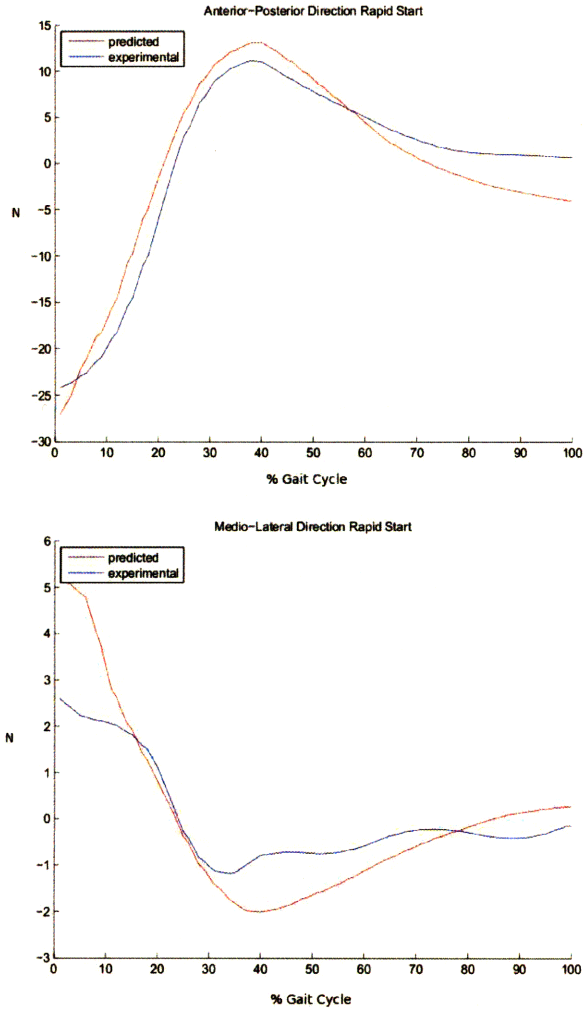


Figure 18: Single Subject Data: The anterior-posterior direction shows good agreement between the predicted and observed data. The medio-lateral direction shows relatively poor agreement between the predicted and experimental data.

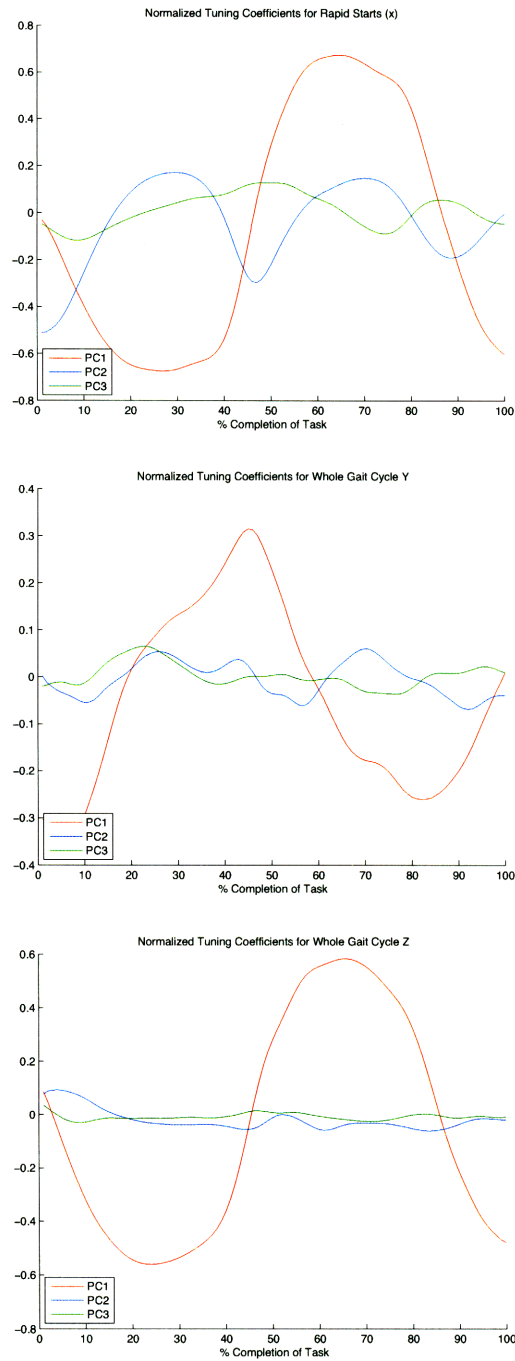


Figure 19: The mean values over all participants and trials of the normalized tuning coefficients associated with a rapid start. From the top to the bottom are the (X), (Y) and (Z) directions, respectively. These normalized tuning coefficients were obtained using Eqn. 13 of Chapter 4.

## CHAPTER 6

### Discussion

#### Is Angular Momentum Regulated during Turning and Rapid Starts?

Whole-body angular momentum is not in general regulated across all movement tasks [6]. For some movements angular momentum is purposefully generated to restore balance, improve stability and maneuverability [14][5][6]. In the case of turning we saw that moments were generated about the  $CM$  by a rotating leg about a pivot foot to complete a turn. For rapid starts, since the desire was to maximize acceleration, the initial left swing leg (foot, shin and ankle) produced a large contribution to the angular momentum about the  $CM$ . In addition, the torso played a role as well, producing large moments in the medio-lateral direction to push the body forward to accelerate quickly.

After foot flat on the second step of the turn the heel rose up concentrating the  $COP$  on the ball of the foot, see Fig. 9. This could be why the  $COP$  and  $CMP$  stay very close during the second step of the turn. The rotation is stable and the difference between the  $CMP$  and  $COP$  is small so the horizontal moments acting on the  $CM$  must also be small. However, in the medio-lateral direction during the turn the GRF predictions indicated a very poor agreement with the zero-moment hypothesis ( $\approx 24\%$ ). This I believe was due to the rotation of the ball of the foot effectively changing the medio-lateral direction in lab frame to the anterior-posterior direction. Instead of there actually being a larger moment being applied to the  $CM$  during the turn. An interesting pilot study would be to look at a plane that changed along with the foot during the turn; essentially a reference that moved with the subject. This way we can continuously assess the forces in the medio-lateral and anterior-posterior direction. At this point I am not sure how to define this plane.

In rapid starts, Fig. 16, the second step shows a high horizontal moment acting about the  $CM$ . For the single subject that was shown here the  $CMP$  was outside of the foot support indicating that a large force was pushing the body over its stance leg1. Unfortunately, we did not have data

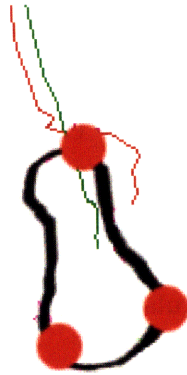


Figure 1: A close-up of the CMP (red) and CP (green) on the first step of a rapid start. The CMP is outside of the approximate region of foot support during stance. This suggests that the moments acting on the CM might have been quite large. Large enough to push the CM outside of foot support.

for the later part of stance because heel strike had occurred off the force plate invalidating the data past single stance. Given the large *CMP* how did the body recover balance in the medio-lateral direction? In the dominant PCs in Fig. 15 the PC for the X direction shows that the limbs corresponding to the left limb are dominant throughout the rapid the rapid start for one full gait cycle.

From these plots I derived a small hypothesis. In the medio-lateral direction there are four main contributions that have similar amounts of contribution to the variance; the upper torso, the chest, the left lower limbs. In this direction the participants swung out their left legs, potentially haphazardly, and destabilized themselves. The upper torso the acts as a balance to restore angular momentum about the CM to normal despite the relatively large moment applied about the CM. Then during rapid starts to improve stability the body purposefully generates moments about the CM with the upper torso to complete the rapid start. This observation sits in line with arguments presented by [6][14]. In the second work it was observed that during certain lateral disturbances the body corrects its CM position to restore stability by purposefully exerting a torque about the CM.

A pilot study looking at this effect might be done in the future to assess the amount of horizontal force is present in a rapid start.

## Participant Independent Measures

The participant independent measures for both turning and rapid starts showed good agreement between different subjects, Chapter 5 Figs. 17, 11. Comparing the rapid start to level ground walking reveals that a similar dimensionality is preserved in similar directions. In [6], the authors reported that four PCs were needed to explain greater than 90% of the data in the medio-lateral direction for level ground walking with a participant-independent analysis. For rapid starts this was also the case. However, it was good that for the participant-dependent analysis that only three PCs were needed for each physiologic direction during a rapid starts. This was surprising given that a rapid start is in some sense more complicated involving more need for postural stability and even moments when the *CP* and *CMP* diverge more than that in level ground straight walking, see Fig. 1. A further study might be done to calculate the degree to which the *CMP* and *CP* diverge during a rapid start. This might be an important factor in developing controls for robotic lower-limb prostheses and bipedal walking machines.

### Comparing the magnitude of whole-body angular momentum in rapid starts and walking

For each direction the absolute magnitude of the whole-body angular momentum was larger for a rapid starts than that observed for fast walking. We saw in the last chapter that the anterior-posterior direction the magnitude was  $< 0.1$  for walking and  $< 0.2$  for a rapid start. The greater amount of angular momentum in this direction can possibly be explained through the passive dynamics of the rocking motion associated with the rapid start versus straight walking. In walking, motions in the medio-lateral directions are more tightly controlled than a more ballistic rapid start. By tightly controlled, we mean that in walking the body does not have to sacrifice some balance in order to produce a fast gait quickly.

In the medio-lateral direction the magnitude of the angular momentum again larger for a rapid start  $< 0.5$  versus walking  $< 0.2$ . This can be explained somewhat through the dynamics of the rapid start. The initial push and control of the anterior-posterior position is much more difficult for a rapid start.

In the transverse plane the obvious thing was again observed and the magnitude of the angular momentum for the rapid start was again larger  $< 0.02$  than walking normally  $< 0.01$ . Again I

believe the nature of the rapid start probably contributed to the relatively larger angular momentum observed for rapid starts versus fast walking.

### **Comparing the magnitude of the whole-body angular momentum in the transverse plane for turning**

As expected the magnitude of the whole-body angular momentum for a turn was larger than that observed for walking. The magnitude for a turn is ten times larger than for walking;  $< 0.1$  for a turn versus  $< 0.01$ . This, in some sense, verifies the laws of physics. Given that the amount of rotation observed in the transverse plane is rather restricted, when someone turns and spins about a foot you expect them to move like a top for a moment in time. However, what is also interesting is that the magnitude is still scaled below 1 indicating that the transverse direction of the turn was still regulated. The body still controls the position of its *CM* very carefully through a turn.

### **Comparing Left and Right Turns - A Pilot Study on Segmental Contributions**

In order to verify what level of similarity exists between left and right handed turn I asked one subject to perform right handed inside turns instead of left handed turns. The results given are depicted in, Fig.2.

The lower limbs again play a dominate role in contributing to angular momentum about the *CM*. This suggests that for healthy subjects conclusions reached for left handed turns will also apply for right handed inside turns.

### First PC of Each Direction of Right Turn – 5 Trials

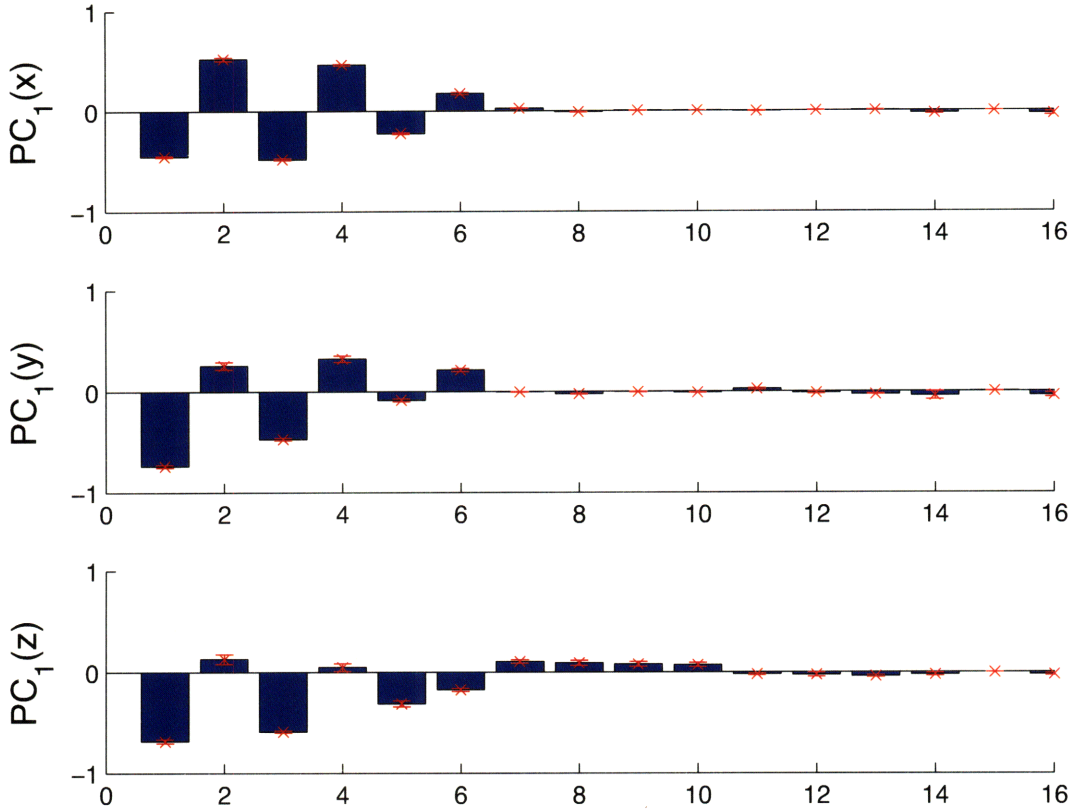


Figure 2: The results of PC analysis on data obtained for a right handed turn. Note that the Z direction shows a similar and opposite contribution from the left and right lower limbs.





## CHAPTER 7

### Conclusion

In this thesis, I showed that the contributions to the whole-body angular momentum remained small through two important transient motions: inside turns and rapid starts. To determine this, I conducted experiments to determine the magnitude and distribution of whole-body angular momentum using an anthropomorphically realistic model. These data were then analyzed using principal component analysis, PCA. From these components, I obtained normalized tuning coefficients that described the times at which specific components were dominant through each transient. This allowed us to understand the strategy during each transient. Where the magnitude of each component indicated a large contribution.

For a left inside turn, we obtained a parsimonious representation of the transverse plane using PCA. This resulted in a dimensionality reduction leaving the three principal components that were needed to explain greater than 90% of the data in a participant-independent analysis and similarly for a participant-dependent analysis. The maximum magnitude of the whole-body angular momentum was  $< 0.1$  that indicated the  $CM$  was regulated throughout the turn-cycle. From an analysis of the segmental contributions to first the principal component in the  $Z$  direction it is clear that the swing leg dominates the turn.

In the case of a rapid start a parsimonious representation was found that included a 3-dimensional representation in the anterior-posterior direction, 4-dimensional representation in the medio-lateral direction, and a 3-dimensional representation in the transverse plane giving a 10-dimensional representation of the  $CM$  in latent angular momentum space. The angular momentum results for a rapid start indicated that the  $CM$  was tightly regulated throughout the rapid start. An analysis of the first principal component in the anterior-posterior direction indicated that first swing leg contributed most to the variance in both the anterior-posterior and medio-lateral directions.

These observations concerning the angular momentum of a rapid start and turn confirm the hypothesis presented at the beginning of this thesis. In particular, that the whole-body angular momentum remains small about the  $CM$ . In addition, that there was large segmental, despite

uneven, cancellation. This work extended hypotheses reported by Herr and Popovic that for a specific transients angular momentum is a conserved quantity.

# Appendix

## Principal Component Analysis Background

Principal component analysis (PCA) [9] is a simple method for reducing the dimensionality of a data set. It is used widely throughout biology, engineering and signal processing. The reason for its popularity is that the method is linear and there exist many fast algorithms to compute the singular value decomposition of a rectangular matrix.

In general, principal component analysis is an orthogonal linear transformation that applies a linear transformation to data that maps it into a new coordinate system. This is done so that the data can be viewed as a linear combination of possibly fewer independent components. The constraint on the linear transformation is the following; the first greatest variance lies on the first axis, known as the first principal component, the second greatest variance on the second axis, and so forth until approximately 100% of the data is explained. PCA is optimal in the least squares sense. That is for the  $L2$  norm the mean-squared- reconstruction-error is minimized.

In general, the optimality in a least-squares sense means the following; Consider the overdetermined system of equations given by,

$$\sum_{j=1}^N X_j \beta_j = y_i,$$

where  $i = 1 \dots m$ . Then the above equation has  $m$  linear equations, given by observations, and  $N$  unknowns  $\beta_1, \beta_2 \dots, \beta_N$ . This was then written in matrix form  $\mathbf{X}\beta = \mathbf{y}$ . Then assuming that the  $N$  columns are linearly independent the solution is given by solving the *Normal Equations*,

$$(\mathbf{X}^T \mathbf{X}) \hat{\beta} = \mathbf{X}^T \mathbf{y}.$$

Our experiment involves a set of observations  $x_1, x_2, \dots, x_N$  that can be represented by a rank- $q$  linear model  $f(\lambda) = \mu + \mathbf{V}_q \lambda$ , where  $\mu$  is a vector in  $\mathbf{R}^p$  that indicates location, and  $\mathbf{V}_q$  is a  $p \times q$  matrix with  $q$  orthogonal unit vectors as columns, and  $\lambda$  is a vector of length  $q$ .

Then to fit the model to the data we minimize the reconstruction error,

$$\min_{\mu, \{\lambda_i\}, \mathbf{V}_q} \sum_{i=1}^N \|x_i - \mu - \mathbf{V}_q \lambda_i\|^2.$$

Then partially optimize the reconstruction error for  $\mu$  and  $\lambda_i$  to get  $\hat{\mu} = \bar{x}$  and  $\hat{\lambda}_i = \mathbf{V}_q^T(x_i - \bar{x})$ . From here our optimization is to find the orthogonal matrix  $\mathbf{V}_q$  that minimizes,

$$\min_{\mathbf{V}_q} \sum_{i=1}^N \|(x_i - \bar{x}) - \mathbf{V}_q \mathbf{V}_q^T(x_i - \bar{x})\|^2.$$

For simplicity assume that the mean of the observations is 0, i.e.  $\bar{x} = 0$ . Then the projection matrix is given by  $\mathbf{H}_q = \mathbf{V}_q \mathbf{V}_q^T$  that maps each observation,  $x_i$  onto its rank- $q$  reconstruction  $\mathbf{H}_q x_i$ , which is the orthogonal projection of  $x_i$  onto the subspace spanned by the columns of  $\mathbf{V}_q$ .

Given a set,  $X$ , of  $N$  observations in  $\mathbf{R}^p$  if  $N > p$  then we can perform a *Singular Value Decomposition* and write,

$$X = UDV^T.$$

Here  $U$  and  $V$  are orthogonal matrices that are  $N \times p$  and  $p \times p$ , respectively. The columns of  $U$  are the left singular vectors, columns of  $V$  are the right singular vectors, and the diagonal elements  $D$  are the singular values. Each solution corresponding to rank  $q$ , that is a solution of  $\mathbf{V}_q$  consists of the first  $q$  columns of  $V$ . The principal components of  $X$  are then the columns of the matrix  $UD$ .

### Lab Specific Considerations for Ground Reference Trajectory Calculations

As mentioned in the experimental methods the holodeck, or MIT gait lab contains two force plates allowing for the analysis of the majority of one full gait cycle. When gait data are analyzed, knowing the entire gait cycle is important for analysis purposes; in particular a gait cycle has two periods of double support with single supports and swing in between each double support period (see [22]).

However, in our setup we are unable to accurately know the COP or CMP for the first double support phase initiating the standard gait cycle; one foot is off of the plate at the beginning of heel strike, Fig 1. The way a gait cycle is determined is by using force plate forces. Therefore, we get that the gait cycle is slightly longer than we expect because toe-off does not fully leave the force

plate until the forward foot is slightly down. In total the measurement of the ground reaction force is impossible for approximately 12 – 15% of the gait cycle<sup>1</sup>. Fortunately, motion capture suffers from no such limitation so full tasks were recorded.

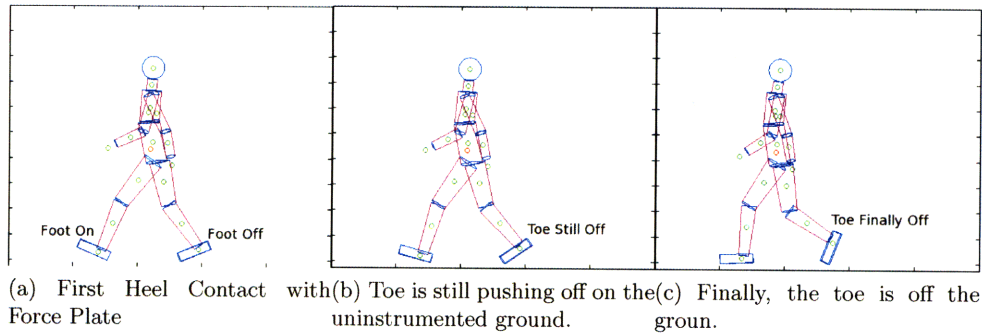


Figure 1: A depiction of the transfer of support during the initial stages of the gait cycle.

Given analog data in the form  $\vec{x}_i \in \mathbb{R}^p$ , where  $p$  is the number output channels and  $i$  is  $1^2 \leq i \leq T$ , with  $T$  is the end time of one gait cycle, we truncated the beginning and end of the trial analog in the following manner;

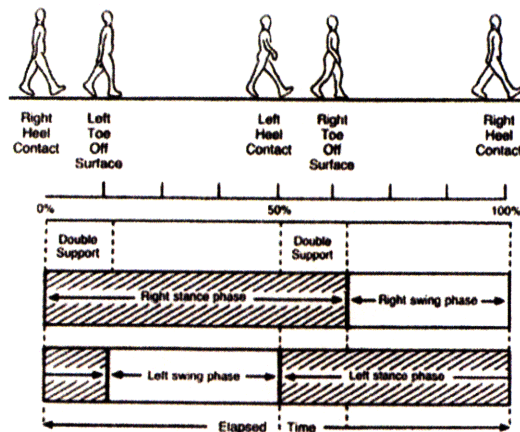


Figure 2: The Normal Gait Cycle. Figure taken from NEJM, 1990.

<sup>1</sup>According to [22] 12% – 15% of the gait cycle is the percentage of double support at the beginning of the normal human gait cycle. If you take heel strike to occur when  $F_z > 10(\text{Newtons})$  in the force plate data.

<sup>2</sup>indexing starts with '1' in matlab and '0' in most common programming languages. I used matlab so I started the index with '1'.

---

**Algorithm 1** Gait Pruning Algorithm for Human Motion Trials

---

```
1:  $FP1_z \leftarrow Z$  force plate 1 analog data,  $FP2_z \leftarrow Z$  force plate 2 analog data
2:  $LToe_z \leftarrow Z$  axis left toe kinematic data,  $RToe_z \leftarrow Z$  axis right toe kinematic data
3:  $idxFP1 \leftarrow$  null vector
4:  $idxFP2 \leftarrow$  null vector
5:  $toeff \leftarrow 0$  //location of toeff after double stance
6:  $range \leftarrow$  determined from heel strike and toe off from force plate
7:  $newRange \leftarrow$  null vector
8: for  $i = 1$  to  $T$ (Length of Trial) do
9:   if  $FP1_z[i] > 10(Newtons)$  then
10:    return  $idxFP2 \leftarrow i$ 
11:   end if
12: end for
13: for  $J = 1$  to  $T$  do
14:   if  $FP2_z[i] > 10(Newtons)$  then
15:    return  $idxFP2 \leftarrow j$ 
16:   end if
17: end for
18:  $minFZ1 \leftarrow min(idxFP1)$ 
19:  $minFZ2 \leftarrow min(idxFP2)$ 
20: if  $minFZ1 \neq minFZ2$  then
21:   Force Plate 1 is the first plate hit
22: else
23:   Force Plate 2 is the first plate hit
24: end if
25:  $lheel \leftarrow$  kinematic data for the left heel
26:  $rlheel \leftarrow$  kinematic data for the right heel
27: if  $lheel \in$  Force Plate 1 then
28:    $toeff \leftarrow doubleSupportFunction(rlheel, rtoe, range)$ 
29: else
30:    $toeff \leftarrow doubleSupportFunction(lheel, ltoe, range)$ 
31: end if
32:  $newRange = (range[1] + toeff) : range[T]$ 
```

---

The above algorithm attempts to take advantage of two things known about the kinematics of gait to determine the approximate time for toe-off directly from marker positions. At a high-level the algorithm starts with a subset of the trial data that starts when the first heel strike occurs on the force plate and ends when the last toe comes off at the end. From the subset the maximum height of the heel marker was found for the foot about to go in swing after the first heel strike. Then further assumptions were made to get closer, for example, in the Double Support Function we used the assumption that during the period of time from heel strike to when the heel is at its highest the heel and toe markers should be far apart if the toe is no longer flat on the ground and in air. This allowed for a better estimate of the position of the toe-off position. However, this has

---

**Algorithm 2** Double Support Function : doubleSupportFunction(heel, toe, range)

---

- 1: Let  $\Delta t$  be a time step, that is approximately 1/120 sec.
  - 2:  $heel_z \leftarrow$  kinematic data for the Z position of the heel of the heel marker
  - 3:  $toe_z \leftarrow$  kinematic data for the Z position of the toe marker
  - 4: Calculate  $\frac{\partial heel_z}{\partial t} \approx \frac{heel_z[i+1] - heel_z[i]}{\Delta t}$
  - 5:  $diffHeelToe \leftarrow$  null vector stores the diff. btwn. the Z coord. of the heel and toe markers.
  - 6: **for**  $i = 1$  to  $T$  **do**
  - 7:   **if**  $(|\frac{\partial heel_z}{\partial t}[i]| - \max(|\frac{\partial heel_z}{\partial t}[i]|)) = 0$  **then**
  - 8:      $diffHeelToe = |toe_z[1, 2, \dots, i] - heel_z[1, 2, \dots, i]|$
  - 9:   **end if**
  - 10: **end for**
- 

problems since it is dependent on marker placement and the participant not bending their toes a great deal during toe-off and entering swing.

To deal with the end of the trial being inaccurate the placement of foot switches might solve the problem so that the location of heel strike is easily noticed.

### Theory of Angular Momentum Primitives

After acquiring sufficiently accurate motion capture data of a human subject performing a transient task, such as turning, we now have run the above model with these data. This produces estimates of each limb's contribution to the total variance observed in the spin angular momentum about the CM. These data are 16 dimensional, one dimension for each segment, which is too large a space to search with many conventional gradient descent algorithms in real-time, so a reduced dimensional model is needed that preserves the dynamics of the biped to develop a controller [5].

To find the basic segments that contribute to the variance seen in the spin angular momentum about the CM we applied a common statistical technique, PCA. Principal Component Analysis (PCA) is applied to each segment treated and treats them as independent components. The human body components were the left and right feet, shins, thighs, hands, forearms, upper arms, upper and lower torso, neck and head. However, after the PCA was applied to the motion capture data while a subject is turning we noticed that there are substantial contributions from the foot that dominated the direction of the turn and the other associated limbs.

This fact is used to develop a balance controller for a bipedal robot to achieve a turn or abrupt start. An *Angular Momentum Primitive*[23] is a principal component obtained from the PC analysis described in the previous paragraph. These components are then used to control a humanoid biped

with a predefined trajectory for the CM. The placement of the feet are determined from the location of the CM by noting the relationship between the CM and the CMP in the definition of the latter point. This effectively constraints the possible location for the CM projection relative to the CMP. This combined with a constraint on the whole-body spin angular momentum allowed us to determine the location of the feet in space relative to the CM.

Then how did we do control? One way which has been used is to control the spin angular momentum about the CM and applying small torques to produce the appropriate stepping behavior [23]. Then each of the angular momentum primitives have a set of hand-tuned gains which can be set in order to produce the first PC more during a part of gait of the second or third resulting in the cumulative behavior described in those particular PCs.

In detail, this amounts to the following application of torque about the CM;

$$\begin{aligned}\vec{\tau}_{des}(\vec{r}_{CM}) &= \dot{\vec{L}}_{des} + \bar{a}\Delta\vec{\theta} + \bar{b}\Delta\dot{\vec{\theta}} \\ &= \dot{\vec{L}}_{des} + \bar{a}\Delta\vec{\theta} + \bar{b}\Delta\vec{L}(\vec{r}_{CM}),\end{aligned}$$

where  $\Delta\vec{L}(\vec{r}_{CM}) = \vec{L}(\vec{r}_{CM}) - \vec{L}_{des}(\vec{r}_{CM})$  and  $\Delta\vec{\theta} = \vec{\theta} - \vec{\theta}_{des}$ , with  $\bar{a}$  and  $\bar{b}$  being second order tensors that represent the rotational stiffness and damping coefficients. Then  $\vec{I}(\vec{r}_{CM}) = \sum_{i=1}^N \vec{I}_i(\vec{r}_{CM})$  is the whole-body moment of the inertia tensor about the CM and  $\vec{\omega} = \vec{I}^{-1}(\vec{r}_{CM})\vec{L}(\vec{r}_{CM})$ .

A good analogy is to think of the robot's CM being controlled by a joy stick and the gains on the different PCs being tuned to produce the desired behavior. An interesting problem is what happens when the PCs for steady-state walking are combine with those for turning? How the knobs, or gains, change as a result? Can we describe a vector algebra of motions in general?



## Bibliography

- [1] Sakagami, Y.; Watanabe, R.; Aoyama, C.; Matsunaga, S.; Higaki, N.; Fujimura, K., "The intelligent ASIMO: system overview and integration," *Intelligent Robots and System, 2002. IEEE/RSJ International Conference on*, pp. 2478-2483 vol.3, 2002
- [2] Au, S. K. and Herr, H. "Initial experimental study on dynamic interaction between an amputee and a powered ankle-foot prosthesis", *Workshop on Dynamic Walking: Mechanics and Control of Human and Robot Locomotion*, Ann Arbor, MI, May 2006.
- [3] Elftman, H. "The function of the arms in walking", *Human Biology* vol. 11, pp. 529-535, 1938
- [4] Vukobratovic, M. and Borovac, B. 2004. "Zero moment point - thirty-five years of its life." *International Journal of Humanoid Robotics* vol.1, num. 1 157-173
- [5] Popovic, MB. Goswami, A. Herr, H 2005. " Ground Reference Points in Legged Locomotion:Definitions, Biological Trajectories and Control Implications " *International Journal of Robotics Research* vol. 24, no. 12, December 2005
- [6] Herr, H. Popovic. M. "Angular momentum in human walking" *Journal of Experimental Biology*, num. 211, 467-481, 2008
- [7] Goswami, A. "Postural Stability of Biped Robots and the Foot-Rotation Indicator (FRI) Point" *International Journal of Robotics Research*, Vol. 18, No. 6, pp. 523-533 June 1999
- [8] Full, R.J. Koditschek, D.E. "Templates and Anchors: Neuromechanical Hypotheses of Legged Locomotion on Land" *Journal of Experimental Biology*, num. 202, 3325 - 3332, 1999
- [9] Hastie, T., Tibshirani, R. Friedman, J. "The Elements of Statistical Learning; Data Mining, Inference and Prediction" (Springer, New York).Weis, I., Voute, P., Schwab, M., et al . (2001)
- [10] Popovic, M., Englehart, A., Herr, H. (2004) "Angular Momentum Primitives for Human Walking: Biomechanics and Control", *Proceedings of 2004 IEEE/RSJ international Conference on Intelligent Robots and Systems*
- [11] Bishop, C. M. 1999. Bayesian PCA. In *Proceedings of the 1998 Conference on Advances in Neural information Processing Systems II* D. A. Cohn, Ed. MIT Press, Cambridge, MA, 382-388.
- [12] Xu, D. and Wang, T., " Lower extremity contributions to altering direction during walking: analysis of angular momentum", *Proceedings on North American Congress on Biomechanics*. University of Waterloo, Waterloo, Ontario, Canada, August 1998

- [13] M . Orendurff , A . Segal , J . Berge , K . Flick , D . Spanier , G . Klute, "The kinematics and kinetics of turning: limb asymmetries associated with walking a circular path", *Gait and Posture* , Volume 23 , Issue 1 , pp.106 - 111, 2005
- [14] A. Hofmann, "Robust Execution of Bipedal Walking Tasks From Biomechanical Principles", PhD Thesis, MIT 2005.
- [15] Arakawa, T. and Fukuda, T. . "Natural motion generation of biped locomotion robot using hierarchical trajectory generation method consisting of GA, EP layers". *Proceedings of the IEEE International Conference on Robotics and Automation*, Albuquerque, NM, pp. 211216.on *Walking Machines*, Bielefeld, Germany. 1997
- [16] Hirai, K., Hirose, M., Haikawa Y., and Takenaka T. "The development of Honda humanoid robot". *Proceedings of the IEEE International Conference on Robotics and Automation*, Leuven, Belgium, pp. 13211326. 1998.
- [17] Dasgupta, A. and Nakamura, Y. Making feasible walking motion of humanoid robots from human motion capture data. *Proceedings of the IEEE International Conference on Robotics and Automation*, Detroit, MI, pp. 4752. 1999.
- [18] Nordin, Frenkel. 2001. *Basic biomechanics of the musculoskeletal system*. 3rd ed. Williams and Wilkins.
- [19] R. Elble, C. Moody, K. Leffler, R. Sinha, "The Initiation of Normal Walking", *Movement Disorders* 1994 , Volume 9 , Issue 2 , Pages 139 - 146.
- [20] K. Hase, R.B. Stein, "Turning Strategies During Human Walking", *Journal of Neurophysiology* 1999, Issue 81, pp. 2914-2922.
- [21] S. Kajita, F. Kanehiro, K. Kaneko, K. Fujiwara, K. Harada, K. Yokoi, H. Hirukawa, "Resolved Momentum Control: Humanoid Motion Planning based on the Linear and Angular Momentum", *Proceedings of the International Conference on Intelligent Robots and Systems* , Las Vegas, Nevada 2003.
- [22] Winter, D.A. "Biomechanics and Motor Control of Human Movement", New York, John Wiley and Sons, 1990
- [23] Popovic M, Englehart A, Herr H. Angular Momentum Primitives for Human Walking: Biomechanics and Control, *IEEE/RSJ International Conference on Intelligent Robots and Systems*; 2004 October; Sendai, Japan.
- [24] Riley, P., Krebs, D. and Popat, R. (1997). Biomechanical analysis of failed sit-to-stand. *IEEE Trans. Rehabil. Eng.* 5, 353-359.
- [25] Hinrichs, R. (1982). Upper extremity function in running. PhD thesis, The Pennsylvania State University, University Park, USA.
- [26] Hinrichs, R. (1987). Upper extremity function in running. II. Angular momentum considerations. *Int. J. Sport Biomech.* 3, 242-263.
- [27] Hinrichs, R. (1992). Case studies of asymmetrical arm action in running. *Int. J. Sport Biomech.* 8, 111-128.
- [28] Hinrichs, R., Cavanagh, P. and Williams, K. (1983). Upper extremity contributions to angular momentum in running. *Biomechanics VIII-B*. Champaign, IL, 641-647.
- [29] Dapena, J. (1978). A method to determine the angular momentum of a human body about three orthogonal axes passing through its center of gravity. *J. Biomech.* 11, 251-256.

- [30] Dapena, J. (1993). An analysis of angular momentum in the discus throw. Paper presented at 14th International Congress of Biomechanics, Paris, France.
- [31] Dapena, J. and McDonald, C. (1989). A three-dimensional analysis of angular momentum in the hammer throw. *Med. Sci. Sports Exerc.* 21, 206-220
- [32] Frohlich, C. (1979). Do spring board divers violate angular momentum conservation? *Am. J. Phys.* 47, 583-592.
- [33] LeBlanc, M. and Dapena, J. (1996). Generation and transfer of angular momentum in the javelin throw. Proceedings of the 20th annual meeting of the American Society of Biomechanics. Atlanta, Georgia, USA, October 17-19, <http://www.elitetrack.com/asbjavelin.pdf>
- [34] King, D. (1999). Generating vertical velocity and angular momentum during skating jumps. Paper presented at 23rd annual meeting of the American Society of Biomechanics, University of Pittsburgh, October, 21-23, <http://asbweb.org/conferences/1990s/1999/ACROBAT/086.PDF>
- [35] Simoneau, G. and Krebs, D. (2000). Whole-body angular momentum during gait: a preliminary study of non-fallers and frequent fallers. *J. Appl. Biomech.* 16, 1-13.
- [36] Wilcoxon, F. (1945). Individual comparisons by ranking methods. *Biometrics* 1, 80- 83.
- [37] M. Farrell, H. Herr, Angular Momentum Primitives for Human Turning: Control Implications for Biped Robots, IEEE - Humanoids Conference, December 2008
- [38] Lacquaniti, F., Grasso, R., Zago, M. (1999) Motor patterns for walking. *News Physiol. Sci.* 14 : 168-174